Inorg. Chem. **2003**, *42*, 4442–4455

Electronic Properties of 4,4′,5,5′-Tetramethyl-2,2′-biphosphinine (tmbp) in the Redox Series *fac*-[Mn(Br)(CO)$_3$(tmbp)], [Mn(CO)$_3$(tmbp)]$_2$, and [Mn(CO)$_3$(tmbp)]$^-$: Crystallographic, Spectroelectrochemical, and DFT Computational Study

František Hartl* and Taasje Mahabiersing

Institute of Molecular Chemistry, Universiteit van Amsterdam, Nieuwe Achtergracht 166, 1018 WV Amsterdam, The Netherlands

Pascal Le Floch,* Francois Mathey, Louis Ricard, and Patrick Rosa

Laboratoire "Hétéroéléments et Coordination", URA CNRS 1499, DCPH, Ecole Polytechnique, 91128 Palaiseau Cedex, France

Stanislav Záliš

J. Heyrovský Institute of Physical Chemistry, Academy of Sciences of the Czech Republic, Dolejškova 3, 182 23 Prague 8, Czech Republic

Received November 25, 2002

Stepwise electrochemical reduction of the complex *fac*-[Mn(Br)(CO)$_3$(tmbp)] (tmbp = 4,4′,5,5′-tetramethyl-2,2′-biphosphinine) produces the dimer [Mn(CO)$_3$(tmbp)]$_2$ and the five-coordinate anion [Mn(CO)$_3$(tmbp)]$^-$. All three members of the redox series have been characterized by single-crystal X-ray diffraction. The crystallographic data provide valuable insight into the localization of the added electrons on the (carbonyl)manganese and tmbp centers. In particular, the formulation of the two-electron-reduced anion as [Mn^0(CO)$_3$(tmbp$^-$)]$^-$ also agrees with the analysis of its IR ν(CO) wavenumbers and with the results of density functional theoretical (DFT) MO calculations on this compound. The strongly delocalized π-bonding in the anion stabilizes its five-coordinate geometry and results in the appearance of several mixed Mn-to-tmbp charge-transfer/IL(tmbp) transitions in the near-UV–vis spectral region. A thorough voltammetric and UV–vis/IR spectroelectrochemical study of the reduction path provided evidence for a direct formation of [Mn(CO)$_3$(tmbp)]$^-$ via a two-electron ECE mechanism involving the [Mn(CO)$_3$(tmbp)]$^\bullet$ radical transient. At ambient temperature [Mn(CO)$_3$(tmbp)]$^-$ reacts rapidly with nonreduced *fac*-[Mn(Br)(CO)$_3$(tmbp)] to produce [Mn(CO)$_3$(tmbp)]$_2$. Comparison with the analogous 2,2′-bipyridine complexes has revealed striking similarity in the bonding properties and reactivity, despite the stronger π-acceptor character of the tmbp ligand.

Introduction

Since the mid-1970s the coordination chemistry of Re(I) carbonyls with chelated α-diimine ligands such as 2,2′-bipyridine (bpy), [Re(L)$_m$(CO)$_{4-m}$(α-diimine)]^n (m = 0−2; n = 0, +1; L = e.g. donor solvent, halide, phosphine), has received wide interest. Many of these complexes have been extensively investigated owing to their electrocatalytic properties in CO_2 reduction[1] and ability to participate in efficient inter- and intramolecular energy- and electron-transfer processes.[2] By contrast, only a few analogous Mn(I) compounds [Mn(L)$_m$(CO)$_{4-m}$(α-diimine)]^n (m = 1−3; n = 0, +1) have been prepared and studied so far, even though

* Authors to whom correspondence should be addressed. E-mail: hartl@science.uva.nl (F.H.); lefloch@poly.polytechnique.fr (P.L.F.).

(1) See for example: (a) Johnson, F. P. A.; George, M. W.; Hartl, F.; Turner, J. J. *Organometallics* **1996**, *15*, 3374−3387. (b) Christensen, P. A.; Hamnett, A.; Muir, A. V. G.; Timney, J. A. *J. Chem. Soc., Dalton Trans.* **1992**, 1455−1463. (c) Calzaferri, G.; Hadener, K.; Li, J. W. *J. Photochem. Photobiol., A* **1992**, *64*, 259−262. (d) Koike, K.; Hori, H.; Ishizuka, M.; Westwell, J. R.; Takeuchi, K.; Ibusuki, T.; Enjouji, K.; Konno, H.; Sakamoto, K.; Ishitani, O. *Organometallics* **1997**, *16*, 5724−5729.

10.1021/ic0206894 CCC: $25.00
Published on Web 06/12/2003

their photochemistry and redox reactivity are equally challenging.[3,4] Whereas light excitation into their metal-to-diimine charge-transfer transitions typically initiates CO-loss and/or isomerization reactions,[3c,d,4a,h,i] their largely diimine-based electrochemical reduction often results in the cleavage of a Mn−L bond.[3g,5] For strongly bound L such as $P(OMe)_3$ or $CNBu^t$ the reversibility of the reduction process increases with the larger substitution number *m*.[4c,5b] In this case, instead, reductive isomerization of the various cis/cis and fac isomers (for given *m*) can occur.[4c,g]

In the Amsterdam group, fundamental studies of the photochemistry, photophysics, and redox properties of transition metal α-diimine carbonyls, including the Re(I) and Mn(I) species,[2d,3,5,6] have recently been extended to the class of coordination compounds with 2,2′-biphosphinine and 1,4-diphospha-1,3-butadiene ligands, the phosphorus equivalents of widely employed 2,2′-bipyridine or 1,4-diaza-1,3-butadiene, respectively. This area is still largely unexplored, even though the coordination chemistry of phosphinines is a rapidly developing field with a promising future.[7] The first joint study with the Palaiseau group[8] focused on the novel intriguing transition metal clusters $[Os_3(CO)_{10-m}(tmbp)(PPh_3)_m]$ ($m = 0, 1$; tmbp = 4,4′,5,5′-tetramethyl-2,2′-biphosphinine, available[9] since 1991). These compounds possess structural, bonding, and physicochemical properties markedly different from those of the analogous clusters with the significantly more basic 2,2′-bipyridine and other α-diimine ligands. Most remarkably, the tmbp ligand is bound in a doubly bridging fashion as dianion to the electron-deficient cluster core with one Os−Os bond split. Differently from the 2,2′-bipyridine derivative, $[Os_3(CO)_{10}(tmbp)]$ is photostable and its electrochemical reduction ultimately results in a CO-loss reaction rather than fragmentation of the cluster core. Obviously, systematic comparative electro- and photochemical investigations of corresponding biphosphinine and bipyridine transition metal complexes are needed to understand the mutual differences and to illustrate the potential of the former compounds in the areas of physical coordination chemistry that have been so far the domain of their α-diimine analogues.

In conformity with this approach, in this article we present results of the combined crystallographic, spectroelectrochemical, and theoretical study of a three-member redox series based on the complex *fac*-$[Mn(Br)(CO)_3(tmbp)]$. The data are compared with those for the corresponding 2,2′-bipyridine complex and its reduction products reported elsewhere.[4c,5,10,11] The synthesis of *fac*-$[Mn(Br)(CO)_3(tmbp)]$ was first described by Mathey and Le Floch in 1996.[12] Its two-electron reduction is shown in this work to produce the anion $[Mn(CO)_3(tmbp)]^-$ that belongs to the remarkable family of formally 16e complexes with five-coordinate geometry stabilized by strong π-bonding in the metallacycle.[13] In the literature $[Mn(CO)_3(tmbp)]^-$ has been identified in the $[Mn_2(CO)_6(tmbp)]$ adduct with the $\{Mn(CO)_3\}^+$ fragment, whose structure has been established by X-ray crystallography.[14] The thorough description of the bonding properties of $[Mn(CO)_3(tmbp)]^-$, supported by the density

(2) See for example: (a) Sun, S. S.; Lees, A. J. *Coord. Chem. Rev.* **2002**, *230*, 171−192. (b) Gabrielsson, A.; Hartl, F.; Smith, J. R. L.; Perutz, R. N. *Chem. Commun.* **2002**, 950−951. (c) Ward, M. D.; Barigelletti, F. *Coord. Chem. Rev.* **2001**, *216*, 127−154. (d) Stufkens, D. J.; Vlček, Jr., A. *Coord. Chem. Rev.* **1998**, *177*, 127−179. (e) Ziessel, R.; Juris, A.; Venturi, M. *Inorg. Chem.* **1998**, *37*, 5061−5069. (f) Yam, V. W. W.; Lau, V. C. Y.; Wang, K. Z.; Cheung, K. K.; Huang, C. H. *J. Mater. Chem.* **1998**, *8*, 89−97. (g) Katz, N. E.; Mecklenburg, S. L.; Meyer, T. J. *Inorg. Chem.* **1995**, *34*, 1282−1284. (h) van Wallendael, S.; Rillema, D. P. *Coord. Chem. Rev.* **1991**, *111*, 297−318.

(3) (a) Staal, L. H.; Oskam, A.; Vrieze, K. *J. Organomet. Chem.* **1979**, *170*, 235−245. (b) Stor, G. J.; van der Vis, M.; Stufkens, D. J.; Oskam, A.; Fraanje, J.; Goubitz, K. *J. Organomet. Chem.* **1994**, *482*, 15−29. (c) Stor, G. J.; Morrison, S. L.; Stufkens, D. J.; Oskam, A. *Organometallics* **1994**, *13*, 2641−2650. (d) Kleverlaan, C. J.; Hartl, F.; Stufkens, D. J. *J. Photochem. Photobiol., A* **1997**, *103*, 231−237. (e) Rossenaar, B. D.; Stufkens, D. J.; Oskam, A.; Fraanje, J.; Goubitz, A. *Inorg. Chim. Acta* **1996**, *247*, 215−229. (f) Andréa, R. R.; de Lange, W. G.; Stufkens, D. J.; Oskam, A. *Inorg. Chem.* **1989**, *28*, 318−323. (g) van der Graaf, T.; Stufkens, D. J.; Oskam, A.; Goubitz, K. *Inorg. Chem.* **1991**, *30*, 599−608.

(4) (a) Carriedo, G. A.; Gimeno, J.; Laguna, M.; Riera, V. *J. Organomet. Chem.* **1981**, *219*, 61−68. (b) Carriedo, G. A.; Carriedo, C.; Crespo, C.; Gómez, P. *J. Organomet. Chem.* **1993**, *452*, 91−96. (c) Brown, N. C.; Carriedo, G. A.; Connelly, N. G.; Garcia Alonso, F. J.; Quarmby, I. C.; Rieger, A. L.; Rieger, P. H.; Riera, V.; Vivanco, M. *J. Chem. Soc., Dalton Trans.* **1994**, 3745−3752. (d) Moya, S. A.; Guerrero, J.; Pastene, R.; Azocar-Guzman, I.; Paredy, A. J. *Polyhedron* **2002**, *21*, 439−444. (e) Bermejo, M. J.; Ruiz, J. I.; Solans, X.; Vinaixa, J. *Inorg. Chem.* **1988**, *27*, 4385−4389. (f) Carlos, R. M.; Carlos, I. A.; Neto, B. S. L.; Neumann, M. G. *Inorg. Chim. Acta* **2000**, *299*, 231−237. (g) Garcia Alonso, F. J.; Riera, V.; Valin, M. L.; Moreiras, D.; Vivanco, M.; Solans, X. *J. Organomet. Chem.* **1987**, *326*, C71−C74. (h) Carriedo, G. A.; Crespo, M. C.; Diaz, C.; Riera, V. *J. Organomet. Chem.* **1990**, *397*, 309−312. (i) Carlos, R. M.; Neumann, M. G. *J. Photochem. Photobiol., A* **2000**, *131*, 67−73.

(5) (a) Hartl, F.; Rossenaar, B. D.; Stor, G. J.; Stufkens, D. J. *Recl. Trav. Chim. Pays-Bas* **1995**, *114*, 565−570. (b) Rossenaar, B. D.; Hartl, F.; Stufkens, D. J.; Amatore, C.; Maisonhaute, E.; Verpeaux, J.-N. *Organometallics* **1997**, *16*, 4675−4685.

(6) Hartl, F.; Aarnts, M. P.; Nieuwenhuis, H. A.; van Slageren, J. *Coord. Chem. Rev.* **2002**, *230*, 107−125.

(7) (a) Mézailles, N.; Mathey, F.; Le Floch, P. *Prog. Inorg. Chem.* **2001**, *49*, 455−550. (b) Dillon, K. B.; Mathey, F.; Nixon, J. F. *Phosphorus: The Carbon Copy. From Organophosphorus to Phospha-organic Chemistry*; Wiley: Chichester, U.K., 1998. (c) Le Floch, P.; Mathey, P. *Coord. Chem. Rev.* **1998**, *179*−*180*, 771−791. (d) Rosa, P.; Sara, X.; Mezailles, N.; Melaimi, M.; Ricard, L.; Mathey, F.; Le Floch, P. *Phosphorus, Sulfur Silicon Relat. Elem.* **2002**, *177*, 1329−1532. (e) Mathey, F. *Rev. Heteroat. Chem.* **1992**, *6*, 1−24.

(8) (a) Bakker, M. J.; Vergeer, F. W.; Hartl, F.; Goubitz, K.; Fraanje, J.; Rosa, P.; Le Floch, P. *Eur. J. Inorg. Chem.* **2000**, 843−845. (b) Bakker, M. J.; Vergeer, F. W.; Hartl, F.; Rosa, P.; Ricard, L.; Le Floch, P.; Calhorda, M. J. *Chem. Eur. J.* **2002**, *8*, 1741−1752.

(9) (a) Le Floch, P.; Carmichael, D.; Richard, L.; Mathey, F. *J. Am. Chem. Soc.* **1991**, *113*, 667−669. (b) Le Floch, P.; Carmichael, D.; Ricard, L.; Mathey, F.; Jutand, A.; Amatore, C. *Organometallics* **1992**, *11*, 2475−2479.

(10) Stor, G. J.; Stufkens, D. J.; Vernooijs, P.; Baerends, E. J.; Fraanje, J.; Goubitz, K. *Inorg. Chem.* **1995**, *34*, 1588−1594.

(11) Hartl, F.; Záliš, S.; Baerends, E. J.; Le Floch, P.; Ricard, L.; Rosa, P. Manuscript in preparation.

(12) Mathey, F.; Le Floch, P. *Chem. Ber.* **1996**, *129*, 263−268.

(13) (a) Liaw, W. F.; Hsieh, C. K.; Lin, G. Y.; Lee, G. H. *Inorg. Chem.* **2001**, *40*, 3468−3475. (b) Lee, C. M.; Lin, G. Y.; Hsieh, C. H.; Hu, C. H.; Lee, G. H.; Peng, S. M.; Liaw, W. F. *J. Chem. Soc., Dalton Trans.* **1999**, 2393−2398. (c) Liaw, W. F.; Lee, C. M.; Lee, G. H.; Peng, S. M. *Inorg. Chem.* **1998**, *37*, 6396−6398. (d) Darensbourg, D. J.; Klausmeyer, K. K.; Reibenspies, J. H. *Inorg. Chem.* **1995**, *34*, 4676−4681. (e) Darensbourg, D. J.; Klausmeyer, K. K.; Reibenspies, J. H. *Inorg. Chem.* **1996**, *35*, 1529−1534. (f) Darensbourg, D. J.; Klausmeyer, K. K.; Reibenspies, J. H. *Inorg. Chem.* **1996**, *35*, 1535−1539. (g) tom Dieck, H.; Rohde, W.; Behrens, U. *Z. Naturforsch.* **1989**, *44*, 158−168. (h) Sellmann, D.; Wille, M.; Knoch, F. *Inorg. Chem.* **1993**, *32*, 2534−2543. (i) Hartl, F.; Vlček, A., Jr.; deLearie, L. A.; Pierpont, C. G. *Inorg. Chem.* **1990**, *29*, 1073−1078. (j) Hartl, F. *Inorg. Chim. Acta* **1998**, *268*, 1−11. (k) Hartl, F.; Stufkens, D. J.; Vlček, A., Jr. *Inorg. Chem.* **1992**, *31*, 1687−1695. (l) Hartl, F.; Barbaro, P.; Bell, I. M.; Clark R. J. H.; Snoeck, T. L.; Vlček, A., Jr. *Inorg. Chim. Acta* **1996**, *252*, 157−166. (m) Aarnts, M. P.; Hartl, F.; Peelen, K.; Stufkens, D. J.; Amatore, C.; Verpeaux, J.-N. *Organometallics* **1997**, *16*, 4686−4695.

functional theoretical (DFT) MO treatment (notably, with ADF2000.2 and Gaussian 98 software packages), has been one of the major goals of this study.

Experimental Section

All reactions and experiments were performed under an atmosphere of dry nitrogen or argon, using Schlenk techniques.

Solvents of analytical grade (all Acros) were freshly distilled from sodium benzophenone (hexane, diethyl ether (Et_2O), tetrahydrofuran (THF), and dimethoxyethane (DME)), sodium wire (toluene), CaH_2 (butyronitrile (PrCN)), and P_2O_5 (CH_2Cl_2). Dioxane-d_6, CD_2Cl_2, and $CDCl_3$ were purchased in sealed ampules, opened in a glovebox, and dried over 4 Å Linde molecular sieves.

The ligand 4,4′,5,5′-tetramethyl-2,2′-biphosphinine (tmbp; **1**) was synthesized according to the reported procedure.[9] The precursor complex $[Mn(CO)_5Br]$ was prepared by bromination of $[Mn_2(CO)_{10}]$, as described elsewhere. Ph_3SnCl (Acros) was purified by sublimation. The supporting electrolyte tetrabutylammonium hexafluorophosphate (Bu_4NPF_6; Aldrich) was recrystallized twice from absolute ethanol and dried overnight under vacuum at 353 K for 12 h before use.

Synthesis of *fac*-[Mn(Br)(CO)$_3$(tmbp)] (2). Toluene (20 mL) was added to $[Mn(CO)_5Br]$ (0.28 g, 1 mmol) and tmbp (**1**) (0.25 g, 1 mmol). The resulting pale yellow solution was heated at 60 °C for 2 h. A precipitate formed during the reaction. It was collected by filtration, washed with hexane (10 mL) and Et_2O (10 mL), and then dried in vacuo. Complex **2** was obtained as a pale-orange solid. Yield: 0.42 g (90%).

CAUTION! The solutions of light-sensitive **2** must be kept in the dark to avoid photochemical decomposition via formation of $[Mn(CO)_3(tmbp)]_2$ (**3**), as was testified by IR spectroscopy. Irradiation of complex **2** (ca. 10^{-2} M) in THF at 293 K with filtered 450 nm light of a medium-pressure Hg lamp results in complete photodecomposition within less than 1 min.

^{31}P NMR ($CDCl_3$): δ 225.1. ^{1}H NMR ($CDCl_3$): δ 2.52 (s, 12H, 4 Me), 8.28 (vd, AA′XX′, 2H, ΣJ(P−H) = 23.3 Hz, $H_{3,3'}$), 8.50 (vd, AA′XX′, 2H, ΣJ(P−H) = 24.8 Hz, $H_{6,6'}$). ^{13}C NMR ($CDCl_3$): δ 22.9 and 24.4 (s, Me), 131.4 (vt, AXX′, ΣJ(P−C) = 49.3 Hz, $C_{3,3'}$), 138.3 (vt, AXX′, ΣJ(P−C) = 29.1 Hz, $C_{5,5'}$ or $C_{4,4'}$), 144.6 (vt, AXX′, ΣJ(P−C) = 21.0 Hz, $C_{4,4'}$ or $C_{5,5'}$), 147.9 (vt, AXX′, ΣJ(P−C) = 16.0 Hz, $C_{6,6'}$), 155.2 (vt, AXX′, ΣJ(P−C) = 64.8 Hz, $C_{2,2'}$), 219.3 (bs, COs). IR (CH_2Cl_2): ν(CO) 2041 (s), 1987 (m), 1950 (m) cm^{-1}. Anal. Calcd for $C_{17}H_{16}BrMnO_3P_2$: C, 43.90; H, 3.47. Found: C, 43.91; H, 3.36.

Synthesis of [Mn(CO)$_3$(tmbp)]$_2$ (3). A solution of sodium naphthalenide (5 mL, 0.4 mmol) in DME was added in a glovebox to complex **2** (186 mg, 0.4 mmol). The resulting red solution was stirred for 5 min. The volume was then reduced, and the solution was left standing overnight. The violet precipitate was then collected by filtration and washed with dry hexane (2 × 5 mL). In order to remove NaBr, complex **3** was extracted with CH_2Cl_2 (5 mL). Heating complex **3** in THF in a sealed tube at 60 °C overnight gave dark-red crystals suitable for X-ray diffraction analysis. Yield: ca. 80%.

^{31}P NMR (dioxane-d_8): δ 248.2. ^{1}H NMR (dioxane-d_8): δ 2.40 and 2.47 (s, 12H, 4 Me), 7.48 (m, AA′XX′, 2H, ΣJ(P−H) = 23.5 Hz, $H_{3,3'}$), 7.90 (m, AA′XX′, 2H, ΣJ(P−H) = 18.0 Hz, $H_{6,6'}$). IR (KBr): ν(CO) 2001 vs, 1958 (s), 1936 (s-m), 1904.5 (s) cm^{-1}. Anal. Calcd for $C_{34}H_{32}Mn_2O_6P_4$: C, 53.01; H, 4.19. Found: C, 52.60; H, 4.35.

Synthesis of [Mn(CO)$_3$(tmbp)]$^-$ (4) as Sodium Salt. A solution of sodium naphthalenide (10 mL, 0.8 mmol) in DME was added in a glovebox to **2** (186 mg, 0.4 mmol). The resulting red-brown solution was stirred for 5 min. The solvent was then removed in vacuo. The red solid obtained was washed with Et_2O (5 mL) and dried overnight at room temperature to sublime off any remaining naphthalene. Single crystals suitable for X-ray diffraction analysis were grown inside a sealed tube filled with a ca. 10 mg of anion **4** in 2 mL of Et_2O, heated to 35 °C on a water bath, and allowed to cool overnight. Yield: ca. 60%. Complex **4** is too air-sensitive to give satisfactory results of elemental analysis.

^{31}P NMR (C_4D_8O): δ 231.30. ^{1}H NMR (C_4D_8O): δ 2.47 and 2.50 (s, 12H, 4 Me), 8.19 (vt, AA′XX′, 2H, ΣJ(P−H) = 25.4 Hz, $H_{3,3'}$), 8.44 (vt, AA′XX′, 2H, ΣJ(P−H) = 17.45 Hz, $H_{6,6'}$). ^{13}C NMR (C_4D_8O): δ 24.3 and 26.1 (s, Me), 122.7 (vt, AXX′, ΣJ(P−C) = 15.3 Hz, $C_{5,5'}$ or $C_{4,4'}$), 126.6 (vt, AXX′, ΣJ(P−C) = 19.7, $C_{3,3'}$ or $C_{6,6'}$), 135.5 (vt, AXX′, ΣJ(P−C) = 20.4 Hz, $C_{6,6'}$ or $C_{3,3'}$), 140.0 (vt, AXX′, ΣJ(P−C) = 11.9 Hz, $C_{5,5'}$ or $C_{4,4'}$), 142.3 (vt, AXX′, ΣJ(P−C) = 73.6 Hz, $C_{2,2'}$), 234.7 (bs, COs).

Synthesis of *fac*-[Mn(SnPh$_3$)(CO)$_3$(tmbp)] (5). Ph_3SnCl (155 mg, 0.4 mmol) was added at room temperature to a solution of anion **4** (0.4 mmol) in DME, prepared as described above. After 10 min, the color of the solution turned red. The solvent was evaporated and the red solid obtained was washed with hexane (3 × 10 mL) and dissolved in CH_2Cl_2 (20 mL). The solution was filtrated over dry Celite and evaporated to dryness to yield analytically pure complex **5**. Yield: 147 mg (50%).

^{31}P NMR (CD_2Cl_2): δ 230.95. ^{1}H NMR (CD_2Cl_2): δ 2.44 and 2.46 (s, 12H, 4 Me of $C_{14}H_{16}P_2$), 6.97−7.17 (m, 15H, H of $SnPh_3$), 8.14 (vd, AA′XX′, 2H, ΣJ(P−H) = 17.0 Hz, $H_{3,3'}$ or $H_{6,6'}$ of $C_{14}H_{16}P_2$), 8.20 (vd, AA′XX′, 2H, ΣJ(P−H) = 23.4 Hz, $H_{6,6'}$ or $H_{3,3'}$ of $C_{14}H_{16}P_2$). ^{13}C NMR (CD_2Cl_2): δ 22.6 (s, Me of $C_{14}H_{16}P_2$), 24.3 (vt, AXX′, ΣJ(P−C) = 9.6 Hz, Me of $C_{14}H_{16}P_2$), 127.5 (s, ^4J(Sn−C) = 10.1 Hz, HC_{para} of $SnPh_3$), 127.7 (s, ^3J(Sn−C) = 41.8 Hz, HC_{meta} of $SnPh_3$), 130.1 (AXX′, ΣJ(P−C) = 12.7 Hz, $C_{3,3'}$ of $C_{14}H_{16}P_2$), 134.4 (AXX′, ΣJ(P−C) = 22.6 Hz, $C_{5,5'}$ or $C_{4,4'}$ of $C_{14}H_{16}P_2$), 136.8 (s, ^2J(Sn−C) =34.5 Hz, HC_{ortho} of $SnPh_3$), 142.1 (AXX′, ΣJ(P−C) = 29.4 Hz, $C_{6,6'}$ of $C_{14}H_{16}P_2$), 143.8 (t, J(P−C) = 1.5 Hz, C_{ipso} of $SnPh_3$), 147.2 (vt, AXX′, ΣJ(P−C) = 12.6 Hz, $C_{4,4'}$ or $C_{5,5'}$ of $C_{14}H_{16}P_2$), 152.0 (vt, AXX′, ΣJ(P−C) = 71.9 Hz, $C_{2,2'}$ of $C_{14}H_{16}P_2$). IR (KBr): ν(CO) 1997 (s), 1932 (s, br) cm^{-1}. MS−IE *m*/*z* (assignment; relative intensity): 734/736 (M^+ for ^{118}Sn and ^{120}Sn; 2), 650/652 ($M^+ - 3CO$ for ^{118}Sn and ^{120}Sn; 4), 377 (100). Anal. Calcd for $C_{35}H_{31}MnO_3P_2Sn$: C, 57.18; H, 4.25. Found: C, 57.05; H, 4.28.

Spectroscopic Measurements. NMR spectra were recorded on a Bruker AC-200 SY spectrometer operating at 200.12 MHz for ^{1}H, 50.32 MHz for ^{13}C, and 81.91 MHz for ^{31}P nuclei. Solvent peaks are used as an internal reference relative to Me_4Si at 0 ppm for the ^{1}H and ^{13}C chemical shifts (ppm); ^{31}P chemical shifts are relative to H_3PO_4 (85%) external reference. All listed coupling constants are in hertz. Abbreviations used: s = singlet, d = doublet, t = triplet, m = multiplet, v = virtual, b = broad. IR spectra were obtained with a Bio-Rad FTS-7 FTIR spectrometer (16 scans, resolution of 2 cm^{-1}), UV−vis spectra with a software-updated Perkin-Elmer Lambda 5 spectrophotometer, and mass spectra with a Shimadzu GC−MS QP 1000 spectrometer (at 70 eV, by the direct inlet method). Elemental analyses were carried out at the "Service d'analyse du CNRS", Gif-sur-Yvette, France.

X-ray Structure Determinations. Crystals of complex **2** were grown by slow evaporation of a dichloromethane solution at room temperature. Dimer **3** was crystallized from THF at 60 °C in a tube sealed under nitrogen. Crystals of extremely air-sensitive anion **4**

(14) Le Floch, P.; Maigrot, N.; Ricard, L.; Charrier, C.; Mathey, F. *Inorg. Chem.* **1995**, *34*, 5070−5072.
(15) Quick, M. H.; Angelici, R. J. *Inorg. Synth.* **1979**, *19*, 160−161, 163.

Table 1. Crystallographic Data and Experimental Parameters for Complexes **2**−**4**

	2	**3**	**4**
formula	$C_{17}H_{16}BrMnO_3P_2$	$C_{34}H_{32}Mn_2O_6P_4$	$C_{25}H_{36}MnNaO_5P_2$
M_w	465.09	770.36	556.41
cryst	red plate	red plate	red plate
cryst size (mm)	0.20 × 0.14 × 0.10	0.20 × 0.16 × 0.07	0.18 × 0.16 × 0.10
cryst syst	monoclinic	monoclinic	triclinic
space group	$P2_1/c$	$C2/c$	$P\bar{1}$
a (Å)	15.1080(5)	22.3415(9)	9.024(5)
b (Å)	12.5770(6)	10.6463(3)	10.130(5)
c (Å)	10.0060(8)	16.0877(7)	15.833(5)
α (deg)	90.00	90.0000(10)	96.830(5)
β (deg)	99.591(3)	118.7330(10)	90.140(5)
γ (deg)	90.00	90.0000(10)	103.770(5)
V (Å^3)	1874.70(19)	3355.4(2)	1395.1(11)
Z	4	4	2
D_{calc} (g cm^{-3})	1.648	1.525	1.325
F_{000}	928	1576	584
μ (cm^{-1})	3.018	0.988	0.635
T (K)	150.0(1)	150.0(1)	150.0(1)
max 2Θ (deg)	60.1	60.0	55.0
hkl ranges	0.21; 0.17; −14.13	−31.16; −14.13; −22.22	−11.11; −11.13; −20.20
reflns collected	5458	10854	9407
indep reflns	5458	4815	6345
reflns included	4559	4221	4643
R_{int}[a]	0.0000	0.0364	0.0340
refinement type	Fsqd	same	same
hydrogen atoms	mixed	same	same
params refined	239	212	343
R1[b]	0.0540	0.0265	0.0459
wR2[c]	0.1541	0.0924	0.1293
criterion	$>2\sigma(I)$	same	same
GOF	1.216	1.145	1.057
diff peak/hole (e Å^3)	0.505(0.094)/ −0.628(0.094)	0.510(0.169)/ −0.533(0.169)	0.768(0.071)/ −0.491(0.071)

[a] $R_{int} = \sum|F_o^2 - F_o^2(\text{mean})|/\sum F_o^2$. [b] The unweighted agreement factor $R1 = \sum||F_o| - |F_c||/\sum|F_o|$. [c] The weighted agreement factor $wR2 = [\sum w(F_o^2 - F_c^2)^2/\sum F_o^4]^{1/2}$, where $w = 1/[\sigma^2(F_o^2) + (xP)^2 + yP]$, $P = (F_o^2 + 2F_c^2)/3$.

were obtained from a solution in diethyl ether, heated at 35 °C overnight in a tube sealed under nitrogen. The tube was broken in a glovebox, and crystals were protected with Paratone oil for handling and submitted to X-ray diffraction analysis. Data were collected on a Nonius Kappa CCD diffractometer using a Mo Kα (λ = 0.71070 Å) X-ray source and a graphite monochromator. Experimental details are presented in Table 1. The crystal structures were solved using SIR 97[16] and SHELXL-97[17] software. ORTEP drawings were made using ORTEP-3 for Windows.[18]

Cyclic Voltammetry. Conventional cyclic voltammograms were recorded with a PAR model 283 potentiostat, using an airtight, light-protected, single-compartment cell placed in a Faraday cage. A Pt disk (0.4 mm diameter) working electrode was polished with a 0.25 μm diamond paste between scans. Coiled Pt and Ag wires served as auxiliary and pseudoreference electrodes, respectively. The concentration of the studied complexes was typically 10^{-3} mol dm^{-3}. Ferrocene (Fc; BDH) or, for complex **3**, cobaltocenium hexafluorophosphate ($Cc^+PF_6^-$; Aldrich) were added as internal standards.[19,20] The position of the ferocene/ferrocenium (Fc/Fc^+) couple toward various reference electrodes can be found elsewhere.[21] For comparison, $E_{1/2}(Cc/Cc^+) = -1.34$ V vs Fc/Fc^+.[20]

IR Spectroelectrochemistry. IR spectroelectrochemical experiments at variable temperatures were carried out with previously described optically transparent thin-layer electrochemical (OTTLE) cells,[22,23] equipped with a Pt minigrid working electrode (32 wires/cm) and CaF_2 windows. Potential control during electrolyses was achieved with a PA4 potentiostat (EKOM, Czech Republic). The solutions were ca. 5×10^{-3} M in complex **2** and contained 3×10^{-1} M Bu_4NPF_6. A thin-layer cyclic voltammogram was recorded in the course of each spectroelectrochemical experiment.

Density Functional Calculations. The ground-state electronic structure of anion **4** was calculated by density functional theory (DFT) methods, using Amsterdam Density Functional (ADF2000.2)[24,25] and Gaussian 98[26] software packages. Within the ADF program Slater-type orbital (STO) basis sets of double-ζ quality with polarization functions for H atoms and triple-ζ quality with additional polarization functions for C, N, O, P, and Mn were employed. Inner shells were represented by the frozen core approximation (1s for C, N, O; 1s, 2s, 2p for P, Mn). Within ADF, the functional used included Becke's gradient correction[27] to the local exchange expression in conjunction with Perdew's gradient correction[28] to local density approximation (LDA) with Vosko−Wilk−Nusair (VWN) parametrization[29] of electron-gas data (ADF/BP). Within Gaussian 98, B3LYP hybrid functionals[30] and the 6-311G** basis set[31] for H, C, N, O, P, and Mn atoms were used (G98/B3LYP). The low-lying excited states of closed-shell complex **4** were calculated using the time-dependent DFT (TD-DFT) method (both ADF/BP and G98/B3LYP). Calculations on **4** were done in constrained C_s symmetry, with the Mn center and C_{ap} positioned in the plane of symmetry.

Results and Discussion

Crystal Structure of *fac*-[Mn(Br)(CO)$_3$(tmbp)] (2). The syntheses of the title biphosphinine complexes **2**−**4** were conducted with the readily available ligand 4,4′,5,5′-tetramethyl-2,2′-biphosphinine (tmbp) **1**. Complex **2** was prepared from equal amounts of **1** and $[Mn(CO)_5Br]$ according to

(16) Altomare, A.; Burla, M. C.; Camalli, M.; Gascarno, G.; Giacovazzo, C.; Guagliardi, A.; Moliterni, A. G. G.; Polidori, G.; Spagna, R. *SIR97*, an integrated package of computer programs for the solution and refinement of crystal structures using single-crystal data, 1999.
(17) Sheldrick, G. M. *SHELXL-97*; Universität Göttingen: Göttingen, 1998.
(18) Farrugia, L. J. ORTEP-3 for Windows. *J. Appl. Crystallogr.* **1997**, *30*, 565.
(19) Gritzner, G.; Kůta, J. *Pure Appl. Chem.* **1984**, *56*, 461−466.
(20) Stojanovic, R. S.; Bond, A. M. *Anal. Chem.* **1993**, *65*, 56−64.
(21) Pavlishchuk, V. V.; Addison, A. W. *Inorg. Chem.* **2000**, *298*, 97−102.
(22) Krejčík, M.; Daněk, M.; Hartl, F. *J. Electroanal. Chem. Interfacial Electrochem.* **1991**, *317*, 179−187.
(23) Hartl, F.; Luyten, H.; Nieuwenhuis, H. A.; Schoemaker, G. *Appl. Spectrosc.* **1994**, *48*, 1522−1528.
(24) Fonseca Guerra, C.; Snijders, J. G.; te Velde, G.; Baerends, E. J. *Theor. Chem. Acc.* **1998**, *99*, 391−403.
(25) van Gisbergen, S. J. A.; Snijders, J. G.; Baerends, E. J. *Comput. Phys. Commun.* **1999**, *118*, 119−138.
(26) Frisch, M. J.; Trucks, G. W.; Schlegel, H. B.; Scuseria, G. E.; Robb, M. A.; Cheeseman, J. R.; Zakrzewski, V. G.; Montgomery, J. A., Jr.; Stratmann, R. E.; Burant, J. C.; Dapprich, S.; Millam, J. M.; Daniels, A. D.; Kudin, K. N.; Strain, M. C.; Farkas, O.; Tomasi, J.; Barone, V.; Cossi, M.; Cammi, R.; Mennucci, B.; Pomelli, C.; Adamo, C.; Clifford, S.; Ochterski, J.; Petersson, G. A.; Ayala, P. Y.; Cui, Q.; Morokuma, K.; Malick, D. K.; Rabuck, A. D.; Raghavachari, K.; Foresman, J. B.; Cioslowski, J.; Ortiz, J. V.; Stefanov, B. B.; Liu, G.; Liashenko, A.; Piskorz, P.; Komaromi, I.; Gomperts, R.; Martin, R. L.; Fox, D. J.; Keith, T.; Al-Laham, M. A.; Peng, C. Y.; Nanayakkara, A.; Gonzalez, C.; Challacombe, M.; Gill, P. M. W.; Johnson, B.; Chen, W.; Wong, M. W.; Andres, J. L.; Gonzalez, C.; Head-Gordon, M.; Replogle, E. S.; Pople, J. A. *Gaussian 98*, revision A.6; Gaussian, Inc.: Pittsburgh, PA, 1998.
(27) Becke, A. D. *Phys. Rev. A* **1988**, *38*, 3098−3100.
(28) (a) Perdew, J. P. *Phys. Rev. B* **1986**, *33*, 8822−8824. (b) Perdew, J. P. *Phys. Rev. B* **1986**, *34*, 7406 (erratum).
(29) Vosko, S. H.; Wilk, L.; Nusair, M. *Can. J. Phys.* **1980**, *58*, 1200.
(30) Stephens, P. J.; Devlin, F. J.; Cabalowski, C. F.; Frisch, M. J. *J. Phys. Chem.* **1994**, *98*, 11623−11627.
(31) Hehre, W. J.; Ditchfield, R.; Pople, J. A. *J. Chem. Phys.* **1972**, *56*, 2257−2261.

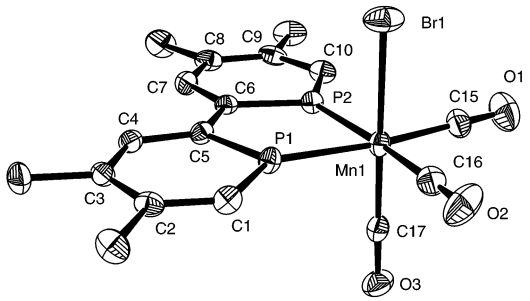

Figure 1. ORTEP drawing of complex **2**. Hydrogen atoms are omitted for clarity. Ellipsoids are scaled to enclose 50% of the electron density. The crystallographic labeling is arbitrary and different from the numbering used for assignment of the ^{13}C NMR signals. Selected bond distances (Å): P1−Mn1, 2.259(1); P2−Mn1, 2.254(1); Mn1−C15, 1.848(4); Mn1−C16, 1.875(4); C15−O1, 1.116(5); C16−O2, 1.083(5); P1−C1, 1.701(4); C1−C2, 1.389(6); C2−C3, 1.409(5); C3−C4, 1.398(5); C4−C5, 1.398(5); C5−C6, 1.470(5); C6−P2, 1.719(4); P2−C10, 1.704(4); C10−C9, 1.392(6); C9−C8, 1.413(6); C8−C7, 1.397(5); C7−C6, 1.396(5). Bond angles (deg): C1−P1−C5, 105.2(2); C6−P2−C10, 105.4(2); P1−Mn1−P2, 79.12(4); P2−Mn1−C15, 92.9(1); C15−Mn1−C16, 94.1(2); C15−Mn1−C17, 87.1(6); C16−Mn1−C17, 87.6(6); C15−Mn1−Br1, 89.3(1); C16−Mn1−Br1, 89.5(1); C16−Mn1−P1, 93.9(1); P1−Mn−Br1, 88.95(4); P2−Mn1−C17, 90.6(6).

eq 1. The fac geometry of **2** can be easily deduced from the ^{31}P NMR spectrum that shows a single resonance at 225.1 ppm. No traces of the mer isomer were detected in the ^{31}P NMR spectrum, which should have produced a classical AB system.

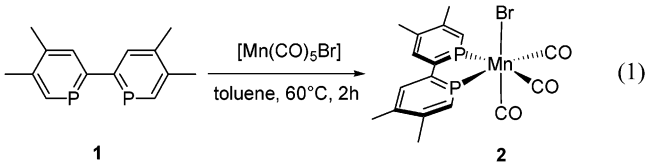

(1)

The ^1H and ^{13}C NMR data of complex **2** also support the proposed structure. Definitive evidence has been given by a single-crystal X-ray diffraction study (Table 1). An ORTEP view of **2** is presented in Figure 1, together with the most significant bond distances and angles. Not unusual for this type of complex, the manganese environment in **2** is nearly perfectly octahedral, with C−Mn−C and P−Mn−C bond angles ranging between 87.1(6)° and 92.9(1)°, respectively. The tmbp ligand in **2** is not significantly distorted compared to its noncoordinate cis form,[9] revealing that its aromaticity has remained preserved. In both cases the internal P−C bonds are slightly longer (e.g., P1−C5 = 1.728(4) Å in **2** and 1.736(4) Å in *cis*-**1**) than the two external ones (P1−C1 = 1.701(4) Å in **2** and 1.716(5) Å in *cis*-**1**). The inter-ring C−C bond lengths are almost identical: 1.470(5) Å in **2** vs 1.490(8) Å in *cis*-**1**. The $Mn-CO_{eq}$ bond lengths are particularly indicative of the strong π-acceptor ability of biphosphinine compared to classical phosphites and 2,2′-bipyridine. Thus, $Mn-C_{eq}$ bond distances in **2** (1.848(4) and 1.875(4) Å) are apparently longer than those found in related complexes *fac*-[Mn(I)$(CO)_3$(bpy)] (1.77(2) and 1.80(2) Å)[10] and *fac*-[Mn(Br)$(CO)_3${$((MeO)_2PO)_2SiMe_2$}] (1.810(4) and 1.832(14) Å).[32] The weaker π-back-bonding toward the two equatorial CO ligands in **2** is also evidenced by a shortening of the CO bonds: 1.083(5) and 1.116(5) Å in **2** compared to 1.14(2) and 1.19(2) Å in *fac*-[Mn(I)$(CO)_3$(bpy)], and 1.122(18) and 1.148(19) Å in the above diphosphite complex.

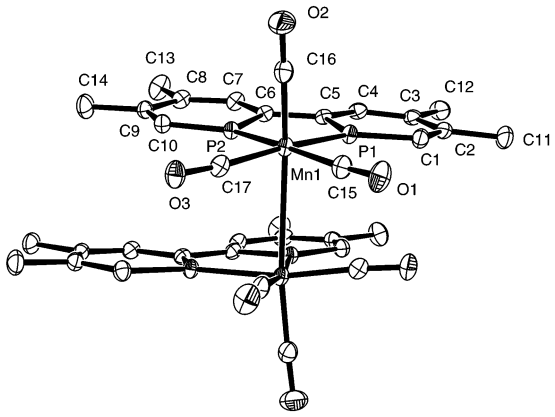

Figure 2. ORTEP drawing of dimer **3**. Hydrogen atoms are omitted for clarity. Ellipsoids are scaled to enclose 50% of the electron density. Selected bond distances (Å): P1−C1, 1.713(2); C1−C2, 1.396(2); C2−C3, 1.409(2); C3−C4, 1.394(2); C4−C5, 1.397(2); C5−C6, 1.459(2); C6−C7, 1.398(2); C7−C8, 1.390(2); C8−C9, 1.417(2); C9−C10, 1.388(2); C10−P2, 1.709(1); P1−Mn1, 2.2362(4); P2−Mn1, 2.2226(4); Mn1−C16, 1.793(2); C16−O2, 1.150(2); Mn1−C15, 1.824(2); C15−O1, 1.147(2); Mn1−C17, 1.814(2); C17−O3, 1.149(2); Mn1−Mn2, 3.0599(5). Bond angles (deg): C6−P2−C10, 104.87(7); C1−P1−C5, 104.55(7); P1−Mn1−P2, 78.69(1); P1−Mn1−C16, 96.96(5); P1−Mn1−C15, 92.91(5); P1−Mn1−C17, 166.45(5); P2−Mn1−C15, 170.25(5); C15−Mn1−C16, 91.18(7); C16−Mn1−C17, 91.75(7).

Crystal Structures of the Reduction Products [Mn$(CO)_3$(tmbp)$_2$]$_2$ (3) and [Mn$(CO)_3$(tmbp)][Na$(OEt_2)_2$] (4). Chemical reduction of complex **2** with 1 molar equiv of sodium naphthalenide in DME at room temperature produces rapidly dimer **3** (eq 2), which was obtained as a poorly soluble dark red solid. The limited solubility precluded recording of a ^{13}C NMR spectrum.

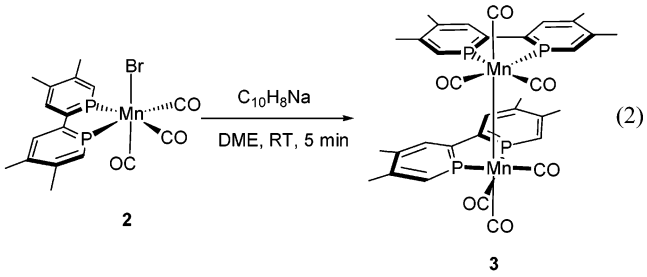

(2)

The dimeric structure of complex **3** could not be established on the simple basis of the available ^1H and ^{31}P NMR data. Again, definitive evidence has been provided by an X-ray crystallographic study (Table 1). Figure 2 presents an ORTEP view of dimer **3**, together with a list of selected of bond lengths and angles. The structure of the dimer resembles that of [$Mn_2(CO)_{10}$].[33] Both tmbp ligands bind as chelates and do not bridge, unlike bridging diphosphine[34] or 2-phosphinyl-phosphinine[35] ligands in dinuclear manganese carbonyls. The coordination geometry of both Mn centers is nearly octahedral. The two equatorial planes are twisted with respect

(32) Sum, V.; Patel, M. T.; Kee, T. P.; Thornton-Pett, M. *Polyhedron* **1992**, *11*, 1743−1754.

(33) (a) Churchill, M. R.; Amoh, K. N.; Wasserman, H. J. *Inorg. Chem.* **1981**, *20*, 1609−1611. (b) Martin, M.; Rees, B.; Mitschler, A. *Acta Crystallogr., Sect. B* **1982**, *38*, 6−15.

to each other, the dihedral angle Θ reaching 40°, similar to $[Mn_2(CO)_{10}]$ with Θ = 50.2°.[33b] Another important comparison concerns the Mn−Mn bond distance, which is rather long in **3** (3.0599(5) Å) compared to $[Mn_2(CO)_{10}]$ (2.895(1) Å). As expected, π-back-bonding to the tmbp ligand in the dimer reduction product is strong. This phenomenon is revealed by elongated internal P−C bond distances (1.735(1) and 1.740(1) Å in **3** compared to 1.728(4) and 1.719(4) Å in **2**), concomitantly with a slightly shortened inter-ring C−C bond distance (1.459(2) Å in **3** vs 1.470(5) Å in **2**) and Mn−P distances (2.2226(4) and 2.2362(4) in **3** compared to 2.254(1) and 2.259(1) Å in **2**). Such differences are in good agreement with the character of the π*(tmbp) lowest unoccupied molecular orbital (LUMO) that is antibonding with regard to the P−C_α bonds and bonding for the inter-ring C−C bond between the two phosphinine rings.[36] Importantly, the apparently longer internal P−C bonds (1.784(1) and 1.788(2) Å) and shorter inter-ring C−C bond (1.440(2) Å) for the noncoordinate radical anion of tmbp ($\mathbf{1}^{\bullet-}$)[37] testify that the tmbp ligand in dimer **3** cannot be viewed as (partly) reduced. The added electrons still largely reside on the Mn centers, being localized in a new σ(Mn−Mn) orbital. Nevertheless, there is crystallographic evidence that delocalization of the Mn−tmbp π-bonding in **3** is not negligible, causing the above-mentioned elongation of the Mn−Mn bond compared to $[Mn_2(CO)_{10}]$, although steric hindrance of the tmbp ligands may also play a role. Similarly to $[Mn_2(CO)_{10}]$, Mn-to-CO π-back-bonding in **3** dominates, being stronger toward the axial than equatorial carbonyls (Mn1−C16, 1.793(2) Å, vs Mn1−C15, 1.824(2) Å).

The reduction of complex **2** with 2 equiv of sodium naphthalenide was again carried out in DME at room temperature (eq 3). In contrast to dimer **3**, the resulting anionic complex $[Mn(CO)_3(tmbp)]^-$ (**4**) is well soluble in DME and THF and could be fully characterized by NMR techniques (^{31}P, ^{1}H, ^{13}C). It should be noted that anion **4** is also readily obtained by reduction of dimer **3** with 2 equiv of sodium naphthalenide.

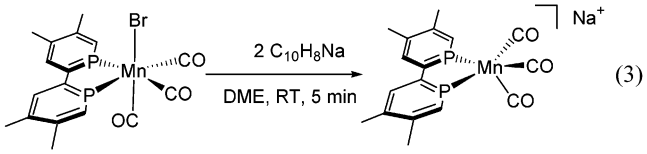

2 **4** (3)

The five-coordinate structure of anion **4** has been unequivocally confirmed by X-ray crystallographic study (Table 1). Suitable crystals of **4** were slowly grown from a diethyl ether solution under strictly inert conditions. An ORTEP view of the sodium salt of **4** is presented in Figure 3, together with a list of the most relevant bond distances and angles. Complex **4** adopts a distorted square pyramidal geometry around Mn. It crystallizes as a coordination polymer, each

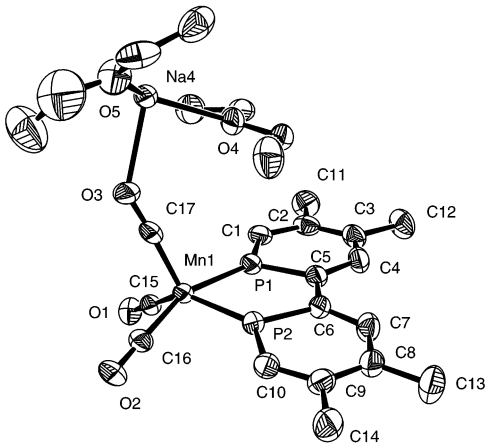

Figure 3. ORTEP drawing of anion **4**. Hydrogen atoms are omitted for clarity. Ellipsoids are scaled to enclose 50% of the electron density. The crystallographic labeling is arbitrary and different from the numbering used for assignment of the ^{13}C NMR signals. Selected bond distances (Å): P1−C1, 1.728(3); C1−C2, 1.376(4); C2−C3, 1.420(4); C3−C4, 1.380(4); C4−C5, 1.398(4); C5−C6, 1.434(4); C6−C7, 1.399(4); C7−C8, 1.383(4); C8−C9, 1.419(4); C9−C10, 1.386(4); C10−P2, 1.728(3); P1−Mn1, 2.180(1); P2−Mn1, 2.201(1); Mn1−C16, 1.773(3); C16−O2, 1.172(3); Mn1−C15, 1.779(3); C15−O1, 1.166(3); Mn1−C17, 1.781(3); C17−O3, 1.167(3); O3−Na4, 2.429(2); O4−Na4, 2.321(2); O5−Na4, 2.286(3). Bond angles (deg): C1−P1−C5, 103.3(1); C6−P2−C10, 103.2(1); P1−Mn1−P2, 78.19(4); P2−Mn1−C16, 88.1(1); P1−Mn1−C15, 116.1(1); C16−Mn1−C17, 94.0(1); C17−Mn1−C15, 95.9(1).

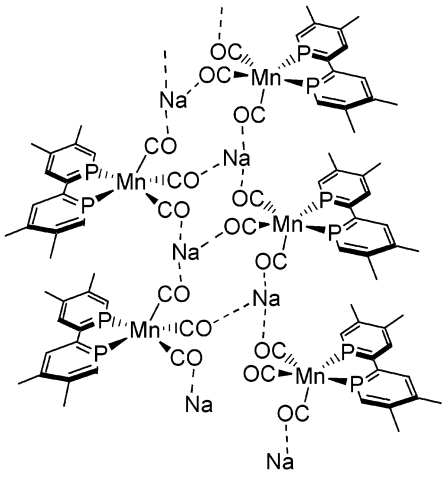

Figure 4. Polymeric arrangement of the sodium salt of anion **4** in the crystal lattice. The two Et_2O ligands at Na^+ have been omitted for clarity.

sodium cation being linked to three carbonyl ligands of three different $[Mn(CO)_3(tmbp)]^-$ molecules. The nearly trigonal bipyramidal coordination sphere of sodium is completed by two diethyl ether ligands. The polymeric structure of anion **4** is schematically shown in Figure 4. A close inspection of bond distances in the tmbp ligand reveals a significant localization of electron density in the π*(tmbp) LUMO. As argued above, occupation of this orbital results in elongated internal P−C bonds (1.751(3) and 1.757(3) Å) and a shortened inter-ring C−C distance (1.434(2) Å), close to the

(34) (a) Reimann, R. H.; Singleton, E. *J. Organomet. Chem* **1972**, *38*, 113−119. (b) Colton, R.; Commons, C. J. *Aust. J. Chem.* **1975**, *28*, 1673−1680. (c) Lemke, F. R.; Kubiak, C. P. *J. Chem. Soc., Chem. Commun.* **1985**, 1729−1730. (d) Morgan, C. A.; Fanwick, P. E.; Rothwell, I. P. *Inorg. Chim. Acta* **1994**, *224*, 105−111.

(35) Waschbüsch, K.; Le Floch, P.; Ricard, L.; Mathey, F. *Chem. Ber./Recl.* **1997**, *130*, 843−849.

(36) Rosa, P.; Ricard, L.; Le Floch, P.; Mathey, F.; Sini, G.; Eisenstein, O. *Inorg. Chem.* **1998**, *37*, 3154−3158.

(37) Choua, S.; Sidorenkova, H.; Berclaz, T.; Geoffroy, M.; Rosa, P.; Mézailles, N.; Ricard, L.; Mathey, F.; Le Floch, P. *J. Am. Chem. Soc.* **2000**, *122*, 12227−12234.

Table 2. Redox Potentials (V vs Fc/Fc^+) of *fac*-[Mn(Br)$(CO)_3$(tmbp)], Its Reduction Products, and Corresponding 2,2′-Bipyridine Complexes[5]

complex [a]	T (K) (solvent)	$E_{p,c}$ [b]	$E_{p,a}$ [c]
[Mn(Br)$(CO)_3$(tmbp)] (**2**)	293 (THF)	−1.67	+0.86
	293 (PrCN)	−1.60	+0.92
	218 (PrCN)	−1.76	+0.92
[Mn(Br)$(CO)_3$(bpy)]	293 (THF)	−1.89	*f*
	223 (THF)	−2.03	*f*
[Mn$(CO)_3$(tmbp)]$_2$ (**3**)[d]	293 (THF)	−1.80	−0.13
[Mn$(CO)_3$(bpy)]$_2$	293 (THF)	−2.05	−0.61
	223 (THF)	−2.21	−0.53
[Mn$(CO)_3$(tmbp)]$^-$ (**4**)	293 (THF)[e]	−2.54[g]	−0.97
	293 (PrCN)	*f*	−0.90
	218 (PrCN)	*f*	−0.76
[Mn$(CO)_3$(bpy)]$^-$	293 (THF)	*f*	−1.53
	223 (THF)	*f*	−1.34

[a] Experimental conditions: cyclic voltammetry (υ = 100 mV/s); 10^{-3} M tmbp complexes; 3×10^{-1} M Bu_4NPF_6 as supporting electrolyte; Pt disk working electrode. $E_{1/2}$ (Fc/Fc^+) = + 0.57 V (THF, 293 K) and +0.42 V (PrCN, 293 K) vs SCE. [b] Cathodic peak potential; irreversible reduction. [c] Anodic peak potential; irreversible oxidation. [d] Produced in situ from [Mn(Br)$(CO)_3$(tmbp)] and Na[Mn$(CO)_3$(tmbp)]. [e] Solution of Na[Mn$(CO)_3$(tmbp)]. [f] Not recorded. [g] Irreversible cathodic wave R2, not shown in Figure 2.

values for noncoordinated radical anion **1**$^{\bullet-}$ (P−C, 1.784(1) and 1.788(2) Å; C−C, 1.440(2) Å)[37] but still significantly different from those for dianion **1**$^{2-}$ (P−C, 1.815(1) and 1.821(3) Å; C−C, 1.401(4) Å).[38] The Mn−P bonds in anion **4** are notably shorter (2.180(1) and 2.201(2) Å) compared to **2** (2.254(1) and 2.259(1) Å) and **3** (2.2226(4) and 2.2362(4) Å). The Mn−C and C−O bond lengths in **4** are quite similar to those observed[39] for the 18e anions [$Mn^{-I}(CO)_5$]$^-$ and [$Mn^{-I}(PR_3)(CO)_4$]$^-$. However, a direct comparison is risky in this case, as the effects of the sodium coordination are difficult to assess with accuracy. (Note that the ν(CO) wavenumbers of Na[Mn$(CO)_3$(tmbp)] are smaller compared to those of Bu_4N[Mn$(CO)_3$(tmbp)] (Table 3), indicating a larger charge on the CO ligands in the sodium salt.) The combined crystallographic data point to the formulation of the two-electron-reduced anion **4** as [$Mn^0(CO)_3$(tmbp$^-$)]$^-$ with a strongly delocalized π-bonding in the Mn(tmbp) metallacycle rather than [$Mn^{-I}(CO)_3$(tmbp)]$^-$ or [$Mn^{I}(CO)_3$(tmbp^{2-})]$^-$. A similar situation is encountered in the square planar complex [Ru^0(tmbp$^-$)$_2$]$^{2-}$ (C−C, 1.436(3) Å; P−C, 1.740(2) Å).[40] Interestingly, the electronic properties of the anionic tmbp ligand in anion **4** are largely preserved in the adduct [$Mn_2(CO)_6$(tmbp)], where the {$Mn(CO)_3$}$^+$ moiety binds to the delocalized five-membered Mn−tmbp metallacycle of [Mn$(CO)_3$(tmbp)]$^-$, with the bond lengths P−C (internal) of 1.760(2) and 1.762(2) Å and C−C (inter-ring) of 1.443(3) Å.[14]

Trapping Reaction of Anion 4 with Ph_3SnCl. Even though a significant part of the charge resides on the tmbp ligand, anion **4** is still sufficiently reactive to undergo reactions with main-group electrophiles. Its trapping reaction with Ph_3SnCl in DME at room temperature yielded the stable red complex [Mn($SnPh_3$)(tmbp)$(CO)_3$] (**5**) (eq 4). All NMR data and elemental analyses have confirmed the proposed formulation. Furthermore, the singlet phosphorus signal in the ^{31}P NMR spectrum of **5** confirms the fac geometry. More detailed physicochemical study of the interesting "inorganometallic" complex **5** was, however, out of the scope of this work.

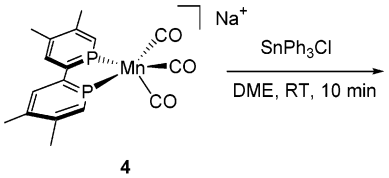

4

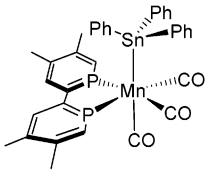

+ NaCl (4)

5

Spectroelectrochemical Study of Complexes 2−4. Chemical reduction of the complex [Mn(Br)$(CO)_3$(tmbp)] (**2**) was shown to produce dimer **3** and anion **4** on overall consumption of 1 and 2 molar equiv, respectively, of the one-electron-reducing agent. However, description of the intimate mechanism of these electron-transfer reactions required more thorough examination. The redox properties and details of the reduction path of complex **2** were investigated by conventional cyclic voltammetry and IR/UV−vis spectroelectrochemistry at variable temperatures. The redox potentials and recorded spectroscopic data (IR ν(CO) wavenumbers and UV−vis absorption maxima) for the studied redox series are presented in Tables 2 and 3, respectively. The corresponding literature data for 2,2′-bipyridine derivatives of complexes **2**−**4** have been added for comparison.

Cyclic Voltammetry. The cyclic voltammogram of complex **2** in THF at 293 K is depicted in Figure 5a. Oxidation of **2** at the potential of the anodic peak O1 is chemically irreversible at moderate scan rates (0.1−20 V/s) in the temperature range 293−218 K. The same result was obtained in butyronitrile. The oxidation was not investigated in detail.

In the cathodic region, the peak R1 belongs to chemically irreversible reduction of complex **2**. Determination[5b,41] of the apparent number of electrons, n_{app}, transferred on the time scale defined by υ = 0.1−20 V/s, was not accurate owing to adsorption of [Mn(Br)$(CO)_3$(tmbp)] at disk ultramicroelectrodes. However, $n_{app} \approx 2$ has been deduced from the analysis of the voltammetric response (see below). No anodic counterpeak (RO1) due to reoxidation of the primary 1e-reduction product, the radical anion [Mn(Br)$(CO)_3$(tmbp)]$^{\bullet-}$ (eq 5), was observed under the above experimental conditions for oxidation. Instead, two other anodic peaks arose on the reverse scan, viz., O2 due to reoxidation of the 2e-reduced anion **4** and, more positively, small O3 due to reoxidation of the 1e-reduced dimer **3** (see Figure 5a). This assignment

(38) Rosa, P.; Mezailles, N.; Ricard, L.; Mathey, F.; Le Floch, P. *Angew. Chem., Int. Ed.* **2001**, *40*, 4476−4479.
(39) (a) Corraine, S. M.; Lai, C. K.; Zhen, Y. Q.; Churchill, M. R.; Buttrey, L. A.; Ziller, J. W.; Atwood, J. D. *Organometallics* **1992**, *11*, 35−40. (b) Riley, P. E.; Davis, R. E. *Inorg. Chem.* **1980**, *19*, 159−165.
(40) Rosa, P.; Mezailles, N.; Ricard, L.; Mathey, F.; Le Floch, P.; Jean, Y. *Angew. Chem., Int. Ed.* **2001**, *40*, 1251−1253.
(41) Amatore, C.; Azzabi, M.; Calas, P.; Jutand, A.; Lefrou, C.; Rollin, Y. *J. Electroanal. Chem. Interfacial Electrochem.* **1990**, *288*, 45−63.

Table 3. IR ν(CO) and UV−Vis Data for *fac*-[Mn(Br)(CO)$_3$(tmbp)] (**2**), Its Reduction Products **3** and **4**, and Corresponding 2,2′-Bipyridine (bpy) Complexes[3b,c,5]

complex	T (K)	ν(CO) (cm^{-1})	λ_{max} (nm) [ϵ_{max} (M^{-1} cm^{-1})]
[Mn(Br)(CO)$_3$(tmbp)] (**2**)	293[a]	2038 (s), 1982 (m), 1944 (m)	310, 368 (sh), 377 [12000], 444 [6000]
	293[a,c]	2041 (s), 1985 (m), 1949 (m)	
	193[b,c]	2041 (s), 1985 (m), 1949 (m)	
[Mn(Br)(CO)$_3$(bpy)]	293[a]	2023 (s), 1935 (m), 1914 (m)	375, 430
	293[a,c]	2021 (s), 1932 (s-m), 1913 (s-m)	273, 357 (sh), 392
	193[b,c]	2027 (s), 1934 (s), 1919 (s)	
[Mn(I)(CO)$_3$(bpy)]	293[a]	2019 (s), 1933 (m), 1916 (m)	385, 445
[Mn(CO)$_3$(tmbp)]$_2$ (**3**)	293[a]	2009 (vs), 1968 (s), 1941 (s-m), 1910 (m)	295sh, 332 (sh), 378 [20000], 431 (sh), 533 [8500]
	293[a,c]	2007 (vs), 1966 (s), 1941 (s-m), 1904 (m)	
	193[b,c]	2007 (vs), 1964 (s),[d] 1905 (m)	
[Mn(CO)$_3$(bpy)]$_2$	293[a,c]	1975 (m), 1963 (w), 1936 (s), 1886 (m), 1866 (m)	395, 455, 650, 740 (sh), 840
	193[b,c]	1974 (m), 1963 (w), 1930 (s), 1877 (m), 1855 (m)	
[Mn(CO)$_3$(tmbp)]$^-$ (**4**)	293[a,e]	1927 (s), 1854 (m), 1814 (m-w)	321, 411 [15000], 540 [2500]
	293[a,f]	1933 (s), 1857 + 1848 (s-m, br)	
	293[a,c]	1928 (s), 1844 (s-m, br)	
	193[b,c]	1926 (s), 1843 (s-m, br)	
[Mn(CO)$_3$(bpy)]$^-$	293[a,c]	1916 (s), 1815 (s, br)	213, 273, 352, 466 (sh), 548, 607 (sh), 676 (sh), 761 (sh)
	193[b,c]	1909 (s), 1811 (s, br)	
	135[g]	1917 (s), 1823 (m), 1815 (sh)	560

[a] In THF. [b] In PrCN. [c] With added supporting electrolyte Bu_4NPF_6 (3×10^{-1} M). [d] Hidden under the band of **4** at 1926 cm^{-1}. [e] As the Na^+ salt with CO···Na^+ interactions (see Figure 3). [f] As the Bu_4N^+ salt. [g] In 2-MeTHF.

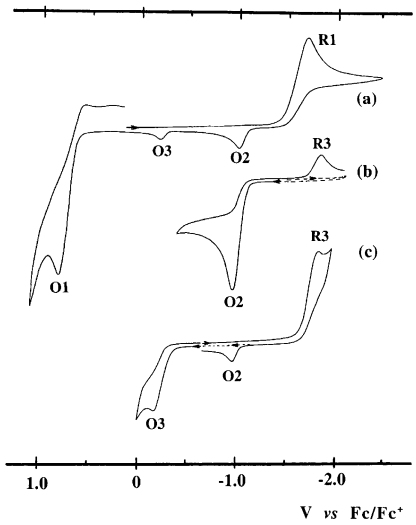

Figure 5. Cyclic voltammograms of parent complex **2** (a) and its reduction products, anion **4** (b) and dimer **3** (c), all in THF. Conditions used: 3×10^{-1} M Bu_4NPF_6 as supporting electrolyte, $T = 293$ K, $\upsilon = 100$ mV s^{-1}, Pt disk microelectrode (0.4 mm diameter),

has been facilitated by recording separately cyclic voltammograms of (i) anion **4** (see Figure 5b), obtained by reduction of complex **2** with Na/Hg, and (ii) dimer **3** (see Figure 5c), formed in situ from equimolar amounts of [Mn(Br)(CO)$_3$(tmbp)] and Na[Mn(CO)$_3$(tmbp)] (precipitated NaBr was filtered off). The results allow us to conclude that the radical anion [Mn(Br)(CO)$_3$(tmbp)]$^{\bullet-}$ is short-lived and rapidly expels the Br$^-$ ligand (eq 6). According to the data in Table 2 (peak potentials R3 vs O2), the electrode potential for the five-coordinate redox couple [Mn(CO)$_3$(tmbp)]$^{\bullet}$/[Mn(CO)$_3$(tmbp)]$^-$ probably lies more positively than that for the six-coordinate redox couple [Mn(Br)(CO)$_3$(tmbp)]$^{\bullet-}$/[Mn(Br)(CO)$_3$(tmbp)]. The radicals [Mn(CO)$_3$(tmbp)]$^{\bullet}$, produced from one-electron-reduced [Mn(Br)(CO)$_3$(tmbp)]$^{\bullet-}$ by fast dissociation of Br$^-$, are therefore instantaneously further reduced at the cathodic potential R1 to give anion **4** (eq 7) and do not concomitantly dimerize to **3**. Instead, dimer **3** is formed by the zero-electron coupling reaction between anion **4** and yet nonreduced complex **2** (eq 8), which was proven in a separate experiment. The latter reaction, however, does not occur on the subsecond time scale of cyclic voltammetry ($\upsilon \geq 100$ mV/s), as indicated by the absence of the cathodic peak due to the reduction of dimer **3** (peak R3 in Figure 5c). The cathodic process R1 in Figure 5a therefore corresponds to the total transfer of two electrons ($n_{app} \approx 2$), resulting in the formation of anion **4** via the ECE sequence as described by eqs 5−7. According to the data in Table 2, the cathodic peak R3 lies 130 mV more negatively than R1 (THF solution, 293 K, $\upsilon = 100$ mV/s). This result implies that the second-order rate constant for the zero-electron coupling reaction following eq 8 must be less than a few hundred M^{-1} s^{-1}.[42] Evidence for the proposed ECE(C)

$$\text{E} \quad [\text{Mn(Br)(CO)}_3\text{(tmbp)}] + \text{e}^- \rightleftharpoons [\text{Mn(Br)(CO)}_3\text{(tmbp)}]^{\bullet-} \tag{5}$$

$$\text{C} \quad [\text{Mn(Br)(CO)}_3\text{(tmbp)}]^{\bullet-} \rightarrow [\text{Mn(CO)}_3\text{(tmbp)}]^{\bullet} + \text{Br}^- \tag{6}$$

$$\text{E} \quad [\text{Mn(CO)}_3\text{(tmbp)}]^{\bullet} + \text{e}^- \rightleftharpoons [\text{Mn(CO)}_3\text{(tmbp)}]^- \tag{7}$$

$$\text{C} \quad [\text{Mn(CO)}_3\text{(tmbp)}]^- + [\text{Mn(Br)(CO)}_3\text{(tmbp)}] \rightarrow [\text{Mn(CO)}_3\text{(tmbp)}]_2 + \text{Br}^- \tag{8}$$

reduction path of complex **2** also comes from IR spectroelectrochemical experiments at variable temperatures, as described hereinafter.

Reduction of dimer **3** at R3 (Figure 5c) produces anion **4**, as revealed by the appearance of the anodic peak O2 on the reverse scan. The intimate mechanism is undoubtedly less simple than described by eq 9, but no detailed study of this process was conducted. The five-coordinate anion **4** is further reduced about 750 mV more negatively than parent complex **2** (Table 2). The cathodic step R2 (not shown in Figure 5)

(42) Nicholson, R. S.; Shain, I. *Anal. Chem.* **1964**, *36*, 706−723.

is chemically completely irreversible, and the corresponding radical product $[Mn(CO)_3(tmbp)]^{2-}$ is probably highly unstable.

$$^1/_2[Mn(CO)_3(tmbp)]_2 + e^- \rightleftharpoons [Mn(CO)_3(tmbp)]^- \quad (9)$$

Reoxidation of anion **4** at O2 results in the recovery of dimer **3**. This is evidenced by the cathodic peak R3 due to the reduction of the dimer that arose during scan reversal beyond O2 (Figure 5b). Obviously, oxidation of **4** produces initially the five-coordinate radicals $[Mn(CO)_3(tmbp)]^\bullet$ (eq 10). Dimer **3** is then formed by two possible coupling reactions. In the first case the radicals $[Mn(CO)_3(tmbp)]^\bullet$ directly dimerize (eq 11). This step, in contrast to the *reduction* path of **2** (in particular eq 7), is essentially possible at the electrode potential O2.

$$[Mn(CO)_3(tmbp)]^- \rightleftharpoons [Mn(CO)_3(tmbp)]^\bullet + e^- \quad (10)$$

$$2[Mn(CO)_3(tmbp)]^\bullet \rightarrow [Mn(CO)_3(tmbp)]_2 \quad (11)$$

Alternatively, the five-coordinate radicals $[Mn(CO)_3(tmbp)]^\bullet$ may first bind a donor solvent molecule (Sv) and convert to the six-coordinate radicals $[Mn(Sv)(CO)_3(tmbp)]^\bullet$ (eq 12). When formed, the latter radicals will directly oxidize at the anodic potential O2 to $[Mn(Sv)(CO)_3(tmbp)]^+$ (eq 13). Similarly to the reduction path of **2**, the cation $[Mn(Sv)(CO)_3(tmbp)]^+$ will then react rapidly with yet nonoxidized anion **4** to give dimer **3** (eq 14). It should be noted that the latter ECEC path (eqs 10 and 12−14) operates in the case of electrochemical oxidation of $[Mn(CO)_3(bpy)]^-$.[5b] In order

$$[Mn(CO)_3(tmbp)]^\bullet + Sv \leftrightarrow [Mn(Sv)(CO)_3(tmbp)]^\bullet \quad (12)$$

$$[Mn(Sv)(CO)_3(tmbp)]^\bullet \rightleftharpoons [Mn(Sv)(CO)_3(tmbp)]^+ + e^- \quad (13)$$

$$[Mn(Sv)(CO)_3(tmbp)]^+ + [Mn(CO)_3(tmbp)]^- \rightarrow [Mn(CO)_3(tmbp)]_2 + Sv \quad (14)$$

to discriminate between the two possible paths producing dimer **3**, the oxidation of anion **4** was studied by cyclic voltammetry in THF at 213 K, and in 2:3 THF/PrCN (v/v) at 293 K. If anion **4** were oxidized via steps 10, 12, and 13, the coupling reaction 14 would be, most likely, sufficiently slow under these conditions[5b] to allow detection of the oxidation products $[Mn(THF)(CO)_3(tmbp)]^+$ and $[Mn(PrCN)(CO)_3(tmbp)]^+$, respectively, on the reverse scan beyond the anodic peak O2 of anion **4** (see Figure 5b). The latter process was also studied in the presence of Bu_4NBr (3×10^{-1} M) at 293 K to form rapidly complex **2** according to eq 15. As argued above for the reduction path, complex **2** will not produce a detectable amount of dimer **3** in reaction with anion **4** (eq 8) at $\upsilon \geq 0.1$ V s^{-1}. However, in all three cases

$$[Mn(Sv)(CO)_3(tmbp)]^+ + Br^- \rightarrow [Mn(Br)(CO)_3(tmbp)] + Sv \quad (15)$$

only the cathodic peak R3 of dimer **3** was observed on the reverse scan beyond the anodic peak O2 (Figure 5b), without any detectable trace of less negatively positioned cathodic peaks due to the reduction of $[Mn(THF)(CO)_3(tmbp)]^+$, $[Mn(PrCN)(CO)_3(tmbp)]^+$, or complex **2**. This result implies that the oxidation of anion **4** yields dimer **3** exclusively via the direct radical coupling reaction (eq 7). In contrast to isoelectronic radicals $[Mn(CO)_3(bpy)]^\bullet$ that form adducts with, e.g., phosphines or coordinating solvent,[3c,5b] the five-coordinate radicals $[Mn(CO)_3(tmbp)]^\bullet$ are less capable of coordinating a Lewis base (eq 12), resembling more $[Mn(CO)_5]^\bullet$ in this regard. This difference may have its origin in the weakly distorted square pyramidal geometry of $[Mn(CO)_3(bpy)]^\bullet$ with axial vacancy having a considerable $4p_z$(Mn) character.[43]

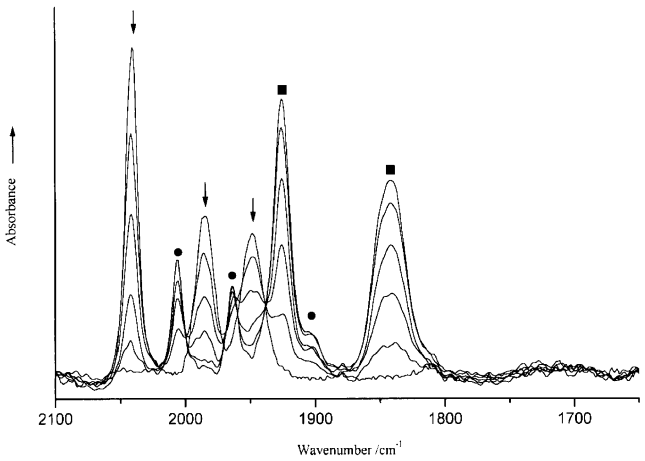

Figure 6. IR spectral changes in the ν(CO) region, recorded in the course of the reduction of complex **2** in PrCN at 193 K within a spectroelectrochemical cell.[23] Symbols used: (↓) complex **2**; (●) dimer **3**; (■) anion **4**.

Finally, oxidation of dimer **3** at the anodic peak O3 in Figures 5a and 5c in the presence of Br^- ions released during the reduction of $[Mn(Br)(CO)_3(tmbp)]$ (eqs 6 and 8) results in the recovery of parent complex **2** (eq 16). This oxidation process, monitored by IR spectroscopy, was separately confirmed by chemical oxidation of $[Mn(CO)_3(tmbp)]_2$ with a ferrocenium salt (PF_6^- or BF_4^-) in THF containing 3×10^{-1} M Bu_4NBr.

$$^1/_2[Mn(CO)_3(tmbp)]_2 - e^- + Br^- \rightleftharpoons [Mn(Br)(CO)_3(tmbp)] \quad (16)$$

IR Spectroelectrochemistry. The ECEC(E) reduction path of complex **2** (eqs 5−8 and 9) can be conveniently followed also in situ with the aid of IR spectroscopy, by monitoring changes in the ν(CO) region during the electrolysis. In butyronitrile at 193 K, the reduction of the parent compound produces directly observable anion **4**, together with some dimer **3** (Figure 6). This result confirms the ECE part of the reduction path described by eqs 5−7. According to the electrode potentials in Table 2, dimer **3** is reduced sufficiently more negatively than complex **2** ($\Delta E_{p,c} = 130$ mV) to exclude observation of anion **4** in the early stage of the electrolysis, in case the latter species is formed via the alternative ECCE reduction path described by eqs 5, 6, 11,

(43) Rosa, A.; Ricciardi, G.; Baerends, E. J.; Stufkens, D. J. *Inorg. Chem.* **1998**, *37*, 6244−6254.

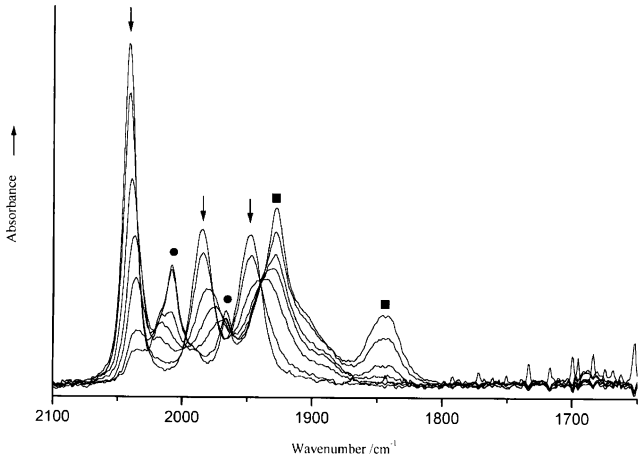

Figure 7. IR spectral changes in the ν(CO) region, recorded in the course of the reduction of complex **2** in PrCN at 293 K within a spectroelectrochemical cell.[22] Symbols used: (↓) complex **2**; (●) dimer **3**; (■) anion **4**.

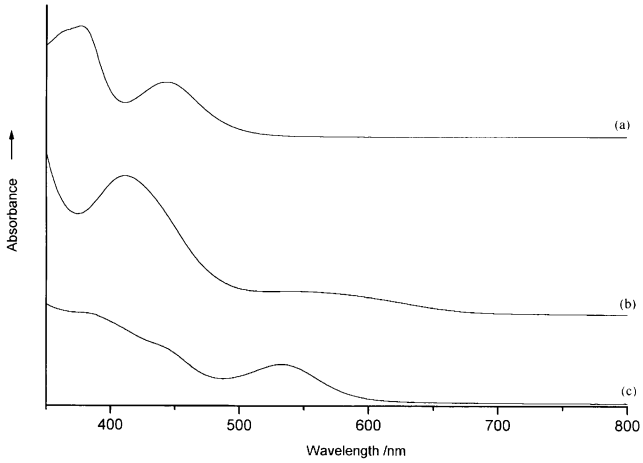

Figure 8. UV−vis spectra of parent complex **2** (a) and its reduction products, anion **4** (b) and dimer **3** (c), all in THF at 293 K.

and 9. The cathodic step (eq 9) indeed occurs at the end of the electrolysis of **2**, when the potential of the working electrode reached the value of the cathodic peak R3 (Figure 5). Apparently, the thermal coupling reaction 8 is significantly inhibited at 193 K, although not completely, resulting in coexistence of all three members of the redox series, precursor **2**, dimer **3**, and anion **4**, in the electrolyzed solution.

In butyronitrile at 243 K, anion **4** is also formed *prior* to dimer **3**, but the coupling reaction (eq 8) occurs with a lower activation energy and dimer **3** therefore dominates over anion **4** until the reduction of **3** itself begins (eq 9).

The IR spectroelectrochemical response to the reduction of complex **2** at 293 K is less simple (Figure 7). In agreement with the rapid coupling reaction 8, anion **4** is initially not observed. It only starts to appear due to the subsequent reduction of dimer **3** at the cathodic wave R3. It is noteworthy that during its reduction the ν(CO) bands of complex **2** become broadened and shift to smaller wavenumbers. This feature is even more pronounced in THF. It may reflect an interaction of complex **2** with a reduced species, probably dimer **3**, for the ν(CO) bands of the latter product are also broadened and shifted to larger wavenumbers until complex **2** disappears. Ultimately, dimer **3** is again reduced to anion **4**. However, at 293 K this step also generates some unassigned minor side products absorbing at 2000−1970 cm^{-1} and 1910−1880 cm^{-1}.

To record UV−vis spectra of pure dimer **3** and anion **4**, precursor **2** is preferably rapidly reduced in THF with 1% Na/Hg, with the formation of pure anion **4** (Figure 8b). Mixing of equimolar amounts of anion **4** and nonreduced complex **2** (coupling reaction 8) then gives pure dimer **3** (Figure 8c), as was proved by IR spectroscopy.

Ground-State Structure of the Five-Coordinate Anion $[Mn(CO)_3(tmbp)]^-$ (4). Selected bond distances and angles of anion **4**, calculated and optimized with the ADF2000.2 and Gaussian 98 program packages, are listed together with the corresponding experimental data in Table 4. It is important to note that also the methyl substituents on the tmbp ligand with their steric and electronic influence were included to provide the best model for the description of the

Table 4. Comparison of Selected Experimental and DFT Calculated Bond Lengths (Å) and Angles (deg) in $[Mn(CO)_3(tmbp)]^-$ (**4**)

bond	ADF/BP	G98/B3LYP	exptl[a]
Mn−P	2.202	2.225	2.201
Mn−C $(CO)_{eq}$	1.782	1.758	1.776
Mn−C $(CO)_{ap}$	1.791	1.785	1.781
P1−C1	1.748	1.749	1.728
P1−C5	1.785	1.780	1.754
C1−C2	1.390	1.382	1.381
C2−C3	1.426	1.434	1.420
C3−C4	1.396	1.390	1.382
C4−C5	1.398	1.408	1.398
C5−C6	1.438	1.433	1.434
C−O (CO)	1.174	1.169	1.168
angle	**ADF/BP**	**G98/B3LYP**	**exptl[a]**
P1−Mn−P2	78.2	78.3	78.19
Mn−P1−C1	138.5	138.8	137.6
Mn−P1−C5	118.8	118.0	118.3
P1−C5−C6	112.0	112.7	112.1
P1−C5−C4	120.6	120.3	120.5
C1−P1−C5	102.7	102.9	103.3
P1−C1−C2	124.8	124.9	124.5
C1−C2−C3	122.9	122.7	123.0
C2−C3−C4	122.2	122.2	121.8
C15−Mn−C17	98.8	98.0	95.9

[a] Symmetry-averaged values.

ground-state electronic structure and bonding properties of the complex. Apart from the goal of the density functional theoretical (DFT) study, it is interesting to compare results obtained with both DFT methods to demonstrate their benefits and mutual differences. Table 4 shows that both ADF/BP and G98/B3LYP data describe qualitatively well the experimental geometry determined by X-ray diffraction. The largest discrepancy regards the OC−Mn−CO angles, which may be ascribed to the $CO\cdots Na^+$ interactions in the sodium salt of anion **4** not considered in the theoretical model. ADF/BP overestimates the P1−C5 distance by 0.031 Å, while the other experimental distances are reproduced within 0.02 Å. The G98/B3LYP data are slightly more accurate in description of the crystallographic results. The optimized geometry of **4** was employed in the following single point electronic structure calculations.

Table 5 summarizes the calculated energies and characters of the frontier molecular orbitals of anion **4**. Both theoretical

Table 5. ADF/BP Calculated One-Electron Energies and Percentage Composition of Selected Occupied and Unoccupied Frontier Molecular Orbitals of $[Mn(CO)_3(tmbp)]^-$ (**4**), Expressed in Terms of the Constituent Fragments (%)

MO	*E* (eV)	Mn	tmbp	CO_{ap}	CO_{eq}	character
unoccupied						
30a″	2.18	2 (p_z); 24 (d_{xz})	35	6	27	π* tmbp + d + CO_{eq}
38a′	1.37	3 (p_y); 2 (d_{z^2}); 4 ($d_{x^2-y^2}$); 15 (d_{xy})	60	4	10	π* tmbp + d
29a″	1.33	3 (d_{xz}); 2 (d_{yz})	93		2	π* tmbp
37a′	0.79	1 ($d_{x^2-y^2}$); 1 (d_{xy})	96		1	π* tmbp
occupied						
36a′	−0.94	9 (p_y); 7 (d_{z^2}); 13 ($d_{x^2-y^2}$); 3 (d_{xy})	49	2	16	π* tmbp + d
28a″	−1.50	2 (p_z); 2 (d_{xz}); 40 (d_{yz})	36	11	8	d + π tmbp + CO
35a′	−1.78	4 (p_x); 15 (d_{z^2}); 40 (d_{xy})	12	15	14	d
34a′	−2.29	1 (p_x); 46 (d_{z^2}); 13 ($d_{x^2-y^2}$); 2 (d_{xy})	11	0	25	d + CO_{eq}
27a″	−2.37	2 (p_z); 16 (d_{yz})	71	6	5	π tmbp

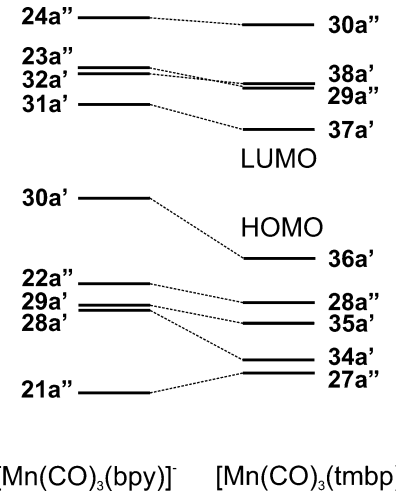

Figure 9. Qualitative molecular orbital diagrams for the isoelectronic anions $[Mn(CO)_3(ChL)]^-$ (ChL = tmbp (**4**) and 2,2′-bipyridine[11]) calculated by the ADF/BP method.

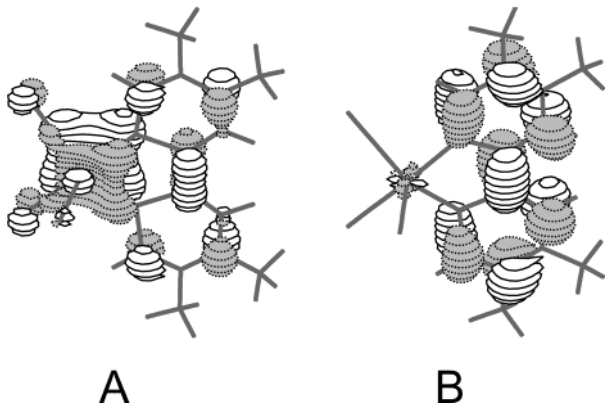

Figure 10. ADF/BP-calculated 37a′ LUMO (A) and 36a′ HOMO (B) of the anion $[Mn(CO)_3(tmbp)]^-$ (**4**).

methods give qualitatively the same composition of the frontier orbitals. Therefore, only the ADF/BP results are discussed below. The ADF/BP qualitative molecular orbital diagram is shown in Figure 9 (right), and the highest occupied and lowest unoccupied molecular orbitals (HOMO and LUMO) are shown in Figure 10. Similar pictures have been obtained for G98/BLY3P.

The 36a′ HOMO of anion **4** (Figure 10B) is strongly delocalized over the Mn(tmbp) metallacycle, having a π-bonding character with 44% contribution of the π_1*(tmbp) LUMO and little contribution (5%) of the π(tmbp) HOMO, the frontier orbitals of free nonreduced tmbp. This means that the two electrons added in the course of the reduction of complex **2** are nearly equally divided between the tmbp ligand and the $\{Mn(CO)_3\}^+$ moiety, producing anion **4**, which can be viewed as $[Mn^0(CO)_3(tmbp^-)]^-$. This localized-valence formulation receives support from X-ray crystallography (see above) and IR spectroscopy. In the latter case, the average CO force constant k_{av} calculated[44] for the Bu_4N^+ salt of anion **4** (about 1420 N m^{-1}, based on data in Table 3) is close to the average k_{av} value for the isoelectronic five-coordinate anions $[Mn^I(CO)_3(DBCat)]^-$ (1498 N m^{-1}; DBCat = 3,5-di-*tert*-butylcatecholate),[13k] and $[Mn^{-I}(CO)_3(dppe)]^-$ (1320 N m^{-1}; dppe = 1,2-diphenylphosphinoethane).[45]

By contrast, the 37a′ LUMO of anion **4** (Figure 10A) is almost exclusively the second lowest unoccupied orbital of free tmbp, π_2*(tmbp). The calculated HOMO−LUMO energy gap (1.73 eV, Table 5) does not deviate much from the experimental potential difference between the electrochemical oxidation and reduction of anion **4** (1.57 V, Table 2); however, solvation effects and the irreversible nature of both redox processes present an obstacle for direct comparison.

The lower-lying occupied orbitals 28a″ (HOMO−1), 35a′ (HOMO−2) and 34a′ (HOMO−3) are predominantly manganese d orbitals, with a significant admixture of a π*(CO) character and contribution from the bonding π(tmbp) orbitals. The higher-lying unoccupied orbitals 29a″ (LUMO + 1) and 38a′ (LUMO + 2) again mainly reside on the π* system of the tmbp ligand, while the 30a″ (LUMO + 3) is highly delocalized over the whole Mn(tmbp) metallacycle.

The strongly delocalized character of the π-bonding between the tmbp ligand and the $\{Mn(CO)_3\}$ moiety in anion **4** is the main factor responsible for the five-coordinate geometry and absence of interaction with Lewis bases (e.g., donor solvents). On the other hand, oxidative addition of electrophiles is facile. As examples may serve reactions with Ph_3Sn^+ or $Mn^+(CO)_3(tmbp)$ (as halide complexes), giving rise to the formation of Sn−Mn and Mn−Mn bonds, respectively. An extraordinary example from the literature is the η^5-bonding between the five-membered Mn(PCCP) metallacycle in anion **4** and the $\{Mn(CO)_3\}^+$ fragment in the dinuclear complex $[Mn_2(CO)_6(tmbp)]$, prepared by a thermal reaction between $[Mn_2(CO)_{10}]$ and tmbp.[14]

(44) Braterman, P. S. *Metal Carbonyl Spectra*; Academic Press: London, 1975.
(45) Kuchynka, D. J.; Amatore, C.; Kochi, J. K. *J. Organomet. Chem.* **1987**, *328*, 133−154.

Table 6. Selected Calculated Singlet Excitation Energies for $[Mn(CO)_3(tmbp)]^-$ (**4**) with Oscillator Strength Larger than 0.005

		ADF/BP		G98/B3LYP		
state	composition[a]	transition energy (eV)	oscillator strength	transition energy (eV)	oscillator strength	exptl transitions (eV)[b]
$^1A'$	94% (36a′ → 37a′)	1.87	0.009	2.20	0.025	2.29
$^1A''$	71% (28a″ → 37a′) 28% (36a′ → 29a″)	2.43	0.003	2.68	0.011	
$^1A''$	61% (36a′ → 29a″) 21% (28a″ → 37a′)	2.72	0.084	2.87	0.094	3.02
$^1A'$	71% (36a′ → 38a′) 22% (28a″ → 29a″)	2.78	0.064	2.93	0.088	
$^1A'$	51% (28a″ → 29a″) 32% (35a′ → 38a′)	3.29	0.091	3.45	0.117	
$^1A'$	55% (35a′ → 38a′) 15% (28a″ → 29a″)	3.60	0.113	3.73	0.117	3.86
$^1A''$	34% (34a′ → 29a″) 24% (27a″ → 38a′)	3.74	0.199	3.92	0.094	

[a] Compositions of electronic transitions are expressed in terms of contributing excitation between ground-state Kohn−Sham molecular orbitals, see Table 5 and Figure 9. [b] Corresponding λ_{max} (nm) values given in Table 3.

Electronic Absorption Spectrum of Anion $[Mn(CO)_3(tmbp)]^-$ (4). The strongly delocalized nature of the π-bonding between the metal carbonyl moiety and the tmbp ligand in anion **4** also determines the character of the low-lying singlet electronic transitions in this complex. The experimental and TD-DFT computed data are summarized in Table 6. Obviously, the theoretical methods reproduce reasonably well the energetic positions and intensities of the absorption bands in the electronic spectrum of anion **4** depicted in Figure 8b. The ADF/BP transition energies are lower by about 0.20−0.35 eV compared to the experimental values, while a fairly good agreement (within 0.10−0.15 eV) has been obtained with G98/BLY3P. The transition energies can be influenced by the surrounding medium, in particular the solvent dipoles that are neglected in the TD-DFT calculations performed on gas-phase molecules at 0 K.

The broad absorption band of relatively low intensity with a maximum at 540 nm is shown to correspond to the lowest-energy singlet electronic transition that is nearly exclusively 36a′ (HOMO) to 37a′ (LUMO) and has a mixed MLCT/IL (IL = tmbp-centered, predominantly π_1*-to-π_2*) character.

The intense asymmetric band at 411 nm belongs mainly to two close-lying allowed electronic transitions, again of mixed MLCT/IL characters: predominantly (61%) 36a′ (HOMO) to 29a″ (LUMO + 1), followed by predominantly (71%) 36a′ (HOMO) to 38a′ (LUMO + 2). Both transitions also have a component that involves excitation from 28a″ (HOMO − 1). An additional, eight to nine times weaker transition, whose main component (71%) involves 28a″ (HOMO − 1) to 37a′ (LUMO) MLCT excitation, is probably responsible for the broadening of the 411 nm band at the low-energy side.

Finally, the intense absorption band at 321 nm (only partly shown in Figure 8b) contains contributions from three allowed combined electronic transitions. They originate in predominantly 28a″ (HOMO − 1), 35a′ (HOMO − 2), and 34a′ (HOMO − 3), respectively, and are directed toward 29a″ (LUMO + 1) and/or 38a′ (LUMO + 2) levels. In general, these three transitions have a prevailing MLCT character, though also the IL (tmbp) component cannot be neglected. This particularly applies for the largely $\pi\pi$*(tmbp) 27a″ (HOMO − 4) to 38a′ (LUMO + 2) orbital excitation as the 24% contribution to the highest lying of the three electronic transitions.

Comparison with Analogous Mn−bpy Complexes. Halide Complexes. Parent complex **2** closely resembles *fac*-$[Mn(X)(CO)_3(bpy)]$ (X = halide, bpy = 2,2′-bipyridne). In the latter halide complexes the π-back-bonding toward the CO ligands is stronger, as revealed by shorter Mn–C and longer C–O bonds for[10] X = I compared to the values for complex **2** (see above), and by their smaller IR CO-stretching wavenumbers (see Table 3). This difference is attributed to the larger π-acceptor capacity of the tmbp ligand compared to 2,2′-bipyridine, encountered also in other pairs of complexes such as[9] $[Cr(CO)_4(ChL)]$ (ChL = tmbp, bpy)]. Indeed, complex **2** is electrochemically reduced about 200 mV less negatively than *fac*-$[Mn(Br)(CO)_3(bpy)]$ (see Table 2). In both cases the LUMO resides predominantly on the π* system of the redox-active ligand, which allows a straightforward comparison.

Both complex **2** and *fac*-$[Mn(X)(CO)_3(bpy)]$ (X = halide) are photoreactive. At room temperature, they produce the corresponding dimers $[Mn(CO)_3(ChL)]_2$ (ChL = tmbp (**3**), bpy) upon irradiation into the lowest-energy absorption bands around 450 nm (Table 3). Whereas the photochemistry of *fac*-$[Mn(X)(CO)_3(bpy)]$ was studied in detail and the formation of the intermediate species $[Mn(Sv)(X)(CO)_2(bpy)]$ (Sv = donor solvent) and *mer*-$[Mn(X)(CO)_3(bpy)]$ along the reaction pathways toward $[Mn(CO)_3(bpy)]_2$ has been firmly established,[3c−e] for complex **2** only preliminary data are available. Time-resolved and temperature-dependent studies need to be conducted to prove whether photoinduced CO-loss and isomerization reactions occur *prior* to the formation of dimer **3** also in this case. The similar bonding properties of complex **2** and *fac*-$[Mn(Br)(CO)_3(bpy)]$ are also reflected in the identical reduction pathways. In both cases, no corresponding transient radical anionic complexes were detected; the axial Br^- ligand is expelled readily, probably due to a "charge leakage" from the reduced chelating ligand (ChL) to the metal−halide bond.[46] Apparently, in the six-coordinate complexes the strong π-acceptor character is only confined to the neutral tmbp ligand. The initial cathodic process consumes two electrons, as the Br^- cleavage reaction is coupled to the concomitant one-electron reduction of the five-coordinate radical transients.

Dimers. Even though the crystal structure of $[Mn(CO)_3(bpy)]_2$ is not available to allow direct comparison with dimer **3** in the solid state, some remarks can be made on the grounds of the IR and UV−vis spectra (see Table 3). The structure of the two dimers in solution is not completely identical, as testified by the different IR ν(CO) patterns. For $[Mn(CO)_3(bpy)]_2$ the geometry is close to eclipsed (C_{2v}; five ν(CO) bands identified). The related dimer *trans,cis*-$[Ru(Me)(CO)_2$-

(46) Klein, A.; Vogler, C.; Kaim, W. *Organometallics* **1996**, *15*, 236−244.

$(iPr\text{-}DAB)]_2$ (iPr-DAB = *N*,*N*′-diisopropyl-1,4-diaza-1,3-butadiene) is also eclipsed in solution (three (plus one very weak) ν(CO) bands identified), but turns nearly anti-eclipsed in the solid state, and the Ru-to-CO π-back-bonding becomes considerably weaker.[47a] Dimer **3** preserves the ν(CO) pattern in solution, but the corresponding wavenumbers increase by 5−10 cm^{-1}. These data point to a less staggered geometry compared to the solid state. The stronger metal-to-diimine and weaker metal-to-CO π-back-bonding in the eclipsed geometry probably originates from a more pronounced overlap between the π^+ and π^- combinations of the occupied d_π(metal) and empty π*(α-diimine) orbitals.[47a] The UV−vis spectra of $[Mn(CO)_3(bpy)]_2$ and *trans,cis*-$[Ru(Me)(CO)_2(iPr\text{-}DAB)]_2$ exhibit a characteristic intense metal-to-diimine charge-transfer band at a low energy (λ_{max} = 840 and 745 nm, respectively)[3c,5a,47a] that is indicative of the strong π-interaction between the coplanar α-diimine ligands in the (nearly) eclipsed geometry.[47a] In the UV−vis spectrum of dimer **3** (Figure 8c), such a band is present at a higher energy (λ_{max} = 533 nm), which is in qualitative agreement with a larger difference between its oxidation and reduction potentials compared to the other two dimers.[5a,47] This difference may point to a more staggered geometry of dimer **3**, presumably due to a steric hindrance between the tmbp ligands that causes their mutual displacement (Figure 2) and is partly responsible for the fairly long Mn−Mn distance (see above). On the other hand, care must be taken when comparing electronic spectra of analogous bpy and tmbp complexes without a theoretical support, as demonstrated below for $[Mn(CO)_3(bpy)]^-$ and anion **4**.

Similar to the parent halide complexes, the formally neutral tmbp ligand in dimer **3** is clearly a stronger π-acceptor than bpy in $[Mn(CO)_3(bpy)]_2$, which is again reflected in the larger ν(CO) wavenumbers and less negative reduction potential of dimer **3** (Tables 2 and 3). Along the reduction paths, both dimers are formed by a zero-electron coupling reaction between the parent halide complexes and the corresponding two-electron-reduced five-coordinate anions. This reaction could be slowed down, but not completely inhibited, at 193 K in butyronitrile. In the case of the bpy complexes, no dimerization occurs at 135 K in 2-Me-THF.[3c,5b]

Five-Coordinate Anions. The formally 16e anion **4** and its equivalent $[Mn(CO)_3(bpy)]^-$ are the most interesting members of the redox series. Their direct structural comparison is possible, as the crystal structure of $[Mn(CO)_3(bpy)]^-$ has also been solved recently for its unusual $Na^+(bpy)(Et_2O)$ salt.[48] Even though details on the electronic structure of $[Mn(CO)_3(bpy)]^-$ and related five-coordinate complexes will be published in a forthcoming paper,[11] a short synopsis is presented already here.

The anions **4** and $[Mn(CO)_3(bpy)]^-$ show a similar crystal structure, described most accurately as a distorted square pyramid with the chelating ligand at the basis. Their space groups and crystal systems are, however, different ($P2_1/c$ and monoclinic, respectively, for the bpy compound),[48] which is most likely dictated by the different coordination environments of the sodium cations. Like anion **4** (see above), also $[Mn(CO)_3(bpy)]^-$ reacts readily with Ph_3SnCl to afford photoreactive *fac*-$[Mn(SnPh_3)(CO)_3(bpy)]$.[49] Binding of donor solvent molecules (THF, PrCN, DMF) to both anions is, however, prevented. The unfavorable coordination of a sixth donor ligand is attributed to the strongly delocalized π-bonding in the Mn−bpy/tmbp chelate rings. Figure 9 documents that the occupied and empty frontier π and π* orbitals of anion **4** have their counterparts in $[Mn(CO)_3(bpy)]^-$, even though the corresponding energies may differ. The highest occupied and lowest unoccupied molecular orbitals, the 36a′ HOMO and 37a′ LUMO of anion **4** (Table 5) lie at lower energies (by 0.8 and 0.27 eV, respectively) than the corresponding levels of $[Mn(CO)_3(bpy)]^-$, in agreement with the similar differences in the oxidation and reduction potentials of the anions (Table 2). The participation of tmbp in the 36a′ HOMO is slightly smaller than that of bpy in the 30a′ HOMO of $[Mn(CO)_3(bpy)]^-$, viz., 49% vs 57%. On the other hand, the tmbp ligand contributes notably more to the three lower-lying metal-based occupied molecular orbitals. Consequently, the participation of the basal and apical CO ligands in these orbitals is reduced by more than 10% in anion **4**, which nicely corresponds with its larger ν(CO) wavenumbers compared to those of $[Mn(CO)_3(bpy)]^-$ (Table 3). The 31a′ LUMO of $[Mn(CO)_3(bpy)]^-$ is fairly π-delocalized, with 68% bpy contribution,[11] while that of anion **4** resides nearly exclusively on the tmbp ligand (96%). The 36a′ → 37a′ HOMO → LUMO electronic transition in anion **4** therefore obtains a mixed MLCT/IL character, while the corresponding 30a′ → 31a′ excitation for $[Mn(CO)_3(bpy)]^-$ can be assigned as a delocalized $\pi_{ML} \rightarrow \pi^*_{ML}$ transition with a limited charge-transfer character. The assignment of the electronic transitions of the anions **4** and $[Mn(CO)_3(bpy)]^-$ in the near-UV−vis region (Table 2) is qualitatively well supported by the time-dependent DFT calculations. With the exception of the HOMO → LUMO transition and the corresponding lowermost absorption band, the higher-lying electronic transitions of anion **4** (Table 6) show large mixing and the absorption bands cannot be ascribed to any individual excitation. A very similar situation is encountered[11] in the case of $[Mn(CO)_3(bpy)]^-$. The differences in its UV−vis spectrum compared to that of anion **4** (Table 3) arise from a plethora of variables: energies and characters of the occupied and empty frontier orbitals, mixing of electronic transitions and their oscillator strength, and energetic difference between individual excitations.

Concluding, the density functional theory in combination with crystallographic, redox, and spectroscopic data allows thorough analysis of bonding properties and electronic structure of highly delocalized complexes with noninnocent ligands, such as anion **4** with the 4,4′,5,5′-tetramethyl-2,2′-biphosphinine ligand. Interestingly, comparison of the studied series of complexes **2**−**4** with analogous 2,2′-bipyridine

(47) (a) tom Dieck, H.; Rohde, W.; Behrens, U. *Z. Naturforsch.* **1989**, *44b*, 158−168. (b) Hartl, F.; Aarnts, M. P.; Nieuwenhuis, H. A.; van Slageren, J. *Coord. Chem. Rev.* **2002**, *230*, 107−125.

(48) Rosa, P. Ph.D. Thesis, École Polytechnique, Palaiseau, France, 2000.

(49) (a) Andréa, R. R.; de Lange, W. G. J.; Stufkens, D. J.; Oskam, A. *Inorg. Chim. Acta* **1988**, *149*, 77. (b) Andréa, R. R.; de Lange, W. G. J.; Stufkens, D. J.; Oskam, A. *Inorg. Chem.* **1989**, *28*, 318.

compounds has revealed similar bonding properties and redox reactivity, independent of the stronger π-acceptor character of the phosphorus ligand.

Acknowledgment. We are thankful for the financial support provided by the Council for Chemical Sciences of the Netherlands Organization for Scientific Research (CW-NWO), the CNRS, and École Polytechnique. This work is also part of the European collaboration COST Action D14, Project D14/0001/99, supported by Grant No. OC.D14.20 (The Ministry of Education of the Czech Republic).

Supporting Information Available: (a) Figure SI-1 showing the polymeric structure of the $Na^+(OEt_2)_2$ salt of anion **4** (PLATON view). (b) X-ray structure determination for complexes **2**−**4**, including tables of crystal data, atomic coordinates and equivalent isotropic displacement parameters, bond distances and angles for all non-hydrogen atoms, anisotropic displacement parameters, and hydrogen coordinates. Crystallographic data in CIF format. This material is available free of charge via the Internet at http://pubs.acs.org.

IC0206894